Quantum theory of optical bistability without adiabatic elimination

M. D. Reid
Physics Department, University of Waikato, Hamilton, New Zealand
(Received 22 June 1987)

A quantum theory describing N two-level atoms in a coherently driven single-mode optical ring cavity is presented. The usual approximation that one may adiabatically eliminate either the cavity or atomic variables is not made. Hence the results are valid for a range of relative cavity and atomic relaxation rates. The theory is based on the linearized equations derived in the positive P representation. A simple analytical solution is presented, including the effect of detunings, for the steady-state transmitted spectrum. The transmitted intensity and squeezing spectra are discussed.

I. INTRODUCTION

Recent experimental interest and success in measuring quantum fluctuations in optical systems make necessary quantum theories modeling realistic experimental situations. The experiments of Slusher *et al.*,[1] Shelby *et al.*,[2] Maeda, Kumar, and Shapiro,[3] Wu *et al.*,[4] Raizen *et al.*,[5] and Machida, Yamamoto, and Itaya[6] measuring fluctuations in quadrature phases of the field are certainly at the limit where theories predicting quantum fluctuations are testable quantitatively. These experiments have been successful in reducing the noise in one of the quadrature-phase amplitudes below the standard quantum limit ("squeezing").[7–9]

An important theoretical system is an ensemble of two-level atoms in an optical cavity. This is the simplest model for at least two recent landmark experiments—the cavity experiments of Slusher *et al.*[1] and Raizen *et al.*[5] Quantum treatments of optical bistability have been developed by Agarwal *et al.*,[10,11] Lugiato *et al.*,[12–14] Drummond and Walls,[15] and Sargent *et al.*[16] (for a review, see Ref. 17). The first calculation of squeezing in such a system was presented by Lugiato and Strini.[18] Calculations of the squeezing in the field transmitted through a multimode cavity were subsequently carried out by Reid and Walls[19,20] and Holm *et al.*[21,22] Ho, Kumar, and Shapiro[23] have developed a theory to describe multiwave mixing in two-level atoms without a cavity. The theories predict considerable enhancement of squeezing for cavity side modes detuned from the pump. At saturation intensities, the favorable detuning approaches the Rabi frequency.[21] The Stark splitting of the two-level atom provides a mechanism for enhancement of nonlinear coupling between fields at the Rabi frequencies.[20] There has been recent success in obtaining agreement between theory and experiment.[24]

This enhancement of squeezing is also present in a single-mode "low-Q" cavity, where the atomic relaxation rate is much smaller than the cavity relaxation rate.[25] Carmichael[26] had noticed such a low-Q cavity to give better squeezing than the high-Q cavity in the absorptive limit. Good squeezing is predicted at much lower atomic detunings and intensities than possible in the high-Q single-mode cavity situation. The recent work of Raizen *et al.*[5] and Orozco *et al.*[27] gives experimental evidence of vacuum-field splitting,[28,29] an effect occurring at low intensities and for cavities with comparable atomic and cavity decay rates.[26] There is an associated strong squeezing detected in the wings of the spectrum, in agreement with theoretical predictions.[5]

The composite system for two-level atoms in a single-mode cavity gives equations involving five variables. In most theories to date[10–25,30,31] a reduction in the dimensionality is made possible by assuming that the cavity relaxation rate is much greater (low Q) or much smaller (high Q) than the atomic relaxation rates. One may then adiabatically eliminate the fast-decaying variables. Of course one or the other of these adiabatic limits does not always provide the appropriate theory for a given experimental situation. Different physical features are demonstrable in the spectra in either case. The amount of squeezing possible in low-Q or high-Q limits differs significantly, and it is not clear what the behavior will be in a realistic situation of arbitrary relative cavity and atomic relaxation rates.

A first analytical treatment of absorptive optical bistability in two-level atoms without adiabatic elimination has been given recently by Carmichael.[26] He points out an important new feature not present in the high- or low-Q adiabatic limits. This is vacuum-field Rabi splitting,[28,29] a splitting of the first-degenerate excited-energy levels of the cavity-atomic system. Carmichael points out that the splitting may be evidenced in absorptive bistability, provided the field and atomic relaxation rates are of the same order and the cavity cooperativity is sufficiently large. This vacuum-field Rabi splitting occurs in the limit of low-field intensities and is distinct from the usual Stark splitting which occurs at high intensities saturating the atoms.

The case of absorptive bistability is, however, restrictive both from a theoretical and an experimental point of view. For example, designs to reduce fluctuations in a quadrature-phase amplitude generally do better in dispersive situations. In the dispersive case, analytical solutions were thought to be too cumbersome, and numerical methods[5,25] have been used to solve for the transmitted spectrum. Raizen *et al.*[5] have recently reported enhancement of squeezing in regimes of vacuum-field

 ©1988 The American Physical Society

Rabi splitting is dispersive bistability.

In this paper we solve analytically for the transmitted field spectrum in a linearized approximation without adiabatic elimination. The method used to derive the solution is presented in a wide context, since it has a general applicability. We show that, contrary to popular belief, a *simple* analytical solution is possible in the nonadiabatic elimination limit. We say simple because the solution is a straightforward superposition of the results for high-Q and low-Q cavity limits and is no more difficult computationally than either even in the dispersive limit. We use the basic equations derived by Drummond and Walls[15] in the positive P representation.[32] In the original treatment[15] these equations were solved in the high-Q limit. We solve these same equations but for arbitrary Q, showing that the solution for the field spectrum is the same as that obtained in the high-Q limit, but with the various drift and diffusion coefficients becoming frequency dependent. We then point out that these broadband frequency coefficients have been published previously by Sargent *et al.*[16] and relate to the low-Q cavity solutions. The solutions obtained previously by either adiabatically eliminating the atomic or field variables are accessible from the full solution in obvious limits.

The simple form of solution allows some physical insight into the structure of the spectrum. We discuss first the spectra in the high-Q limit where the atomic variables may be eliminated. This is essentially revision of the work published previously although a number of new points are discussed. We provide physical reasons as to why the high-Q cavity limit is less favorable for inducing squeezing. The low-Q cavity limit where the cavity variables are adiabatically eliminated is also presented. The particular structure of the solution encourages us to plot particular coefficients against frequency and hence provides some insight. Good squeezing is possible at the Rabi sidepeaks of the spectrum, for low atomic detunings, because of resonant scattering induced by the Stark splitting. The transmitted intensity and squeezing spectrum for the more general cavity where neither the high-Q nor low-Q adiabatic elimination limits are valid is also discussed. We present explicit solutions for the eigenvalues in the low-intensity limit including nonzero atomic and cavity detunings, and hence discuss where the vacuum-field Rabi splitting is evident. At low intensities squeezing may be enhanced, as already reported and experimentally investigated in the work of Raizen *et al.*, at the vacuum-field Rabi side peaks. We discuss in terms of scattering diagrams the effect of cavity detuning and Q values on the enhancement. Results are also discussed for higher intensities.

II. QUANTUM-MECHANICAL EQUATIONS

We consider an ensemble of N identical two-level atoms in a single-ported optical-ring cavity pumped by an external driving field. The cavity is assumed to be of sufficiently high Q (i.e., the reflectivity of the mirrors is sufficient) that one may assume the mean-field approximation and neglect spatial fluctuations. We write the following model Hamiltonian in the electric-dipole and rotating-wave approximations:

$$
\begin{aligned}
&H=\sum_{\mu=0}^{4} H_{\mu} \ , \\
&H_0=\hbar\omega_c a^{\dagger}a+\tfrac{1}{2}\sum_{i=1}^{N}\hbar\omega_0\sigma_{zi} \ , \\
&H_1=i\hbar g\sum_{i=1}^{N}(\sigma_i a^{\dagger}e^{-ikr_i}-\sigma_i^{\dagger}ae^{ikr_i}) \ , \\
&H_2=i\hbar(a^{\dagger}\varepsilon e^{-i\omega_L t}-a\varepsilon^{*}e^{i\omega_L t}) \ , \\
&H_3=\sum_{i=1}^{N}(\Gamma\sigma_i^{\dagger}+\Gamma^{\dagger}\sigma_i+\Gamma_p\sigma_{zi}) \ , \\
&H_4=a\Gamma_c^{\dagger}+a^{\dagger}\Gamma_c \ .
\end{aligned}
\tag{1}
$$

$a^{\dagger},a$ are the boson creation and annihilation operators, respectively, for the resonant cavity mode of frequency ω_c. $\sigma_i,\sigma_i^{\dagger},\sigma_{zi}$ are the Pauli operators for the ith two-level atom with atomic transition frequency ω_0. g is the electric-dipole coupling constant describing the interaction between the N two-level atoms and the field. The cavity mode a is driven by an external coherent input field ε of frequency ω_L. The reservoirs Γ,Γ_p describe energy loss from the atoms via spontaneous emission and phase damping (e.g., collisional processes), respectively. The dissipation of the cavity field mode through the cavity port is described by the reservoir Γ_c.

Quantum theories of optical bistability using the Hamiltonian (1) have been developed by Agarwal *et al.*,[10] Lugiato,[12] Drummond and Walls,[15] and Sargent *et al.*[16] We use here the method of Drummond and Walls who derive c-number stochastic differential equations in a positive P representation. These equations are the starting point of our paper. For the sake of completeness, we summarize the method used to derive these equations. Firstly, a master equation is derived for the density operator ρ in the Markoffian approximation. Following the technique of Haken,[33] a normally ordered characteristic function is defined and a probability distribution $P(\alpha,\alpha^{\dagger},v,v^{\dagger},D)$ in a five-dimensional complex phase space is then defined in terms of this characteristic function. One thus establishes a correspondence between c numbers and operators as follows:

$$
\begin{aligned}
&v\leftrightarrow S=\sum_{i=1}^{N}\sigma_i e^{-ikr_i} \ , \\
&v^{\dagger}\leftrightarrow S^{\dagger}=\sum_{i=1}^{N}\sigma_i^{\dagger}e^{ikr_i} \ , \\
&D\leftrightarrow S_z=\sum_{i=1}^{N}\sigma_{zi} \ , \\
&\alpha\leftrightarrow a, \quad \alpha^{\dagger}\leftrightarrow a^{\dagger} \ .
\end{aligned}
\tag{2}
$$

The c-number averages defined by the probability distribution P are the averages of the corresponding normally ordered operators. In the representation used v, $v^{\dagger},\alpha$, $\alpha^{\dagger}$, and D are independent complex variables. This is in contrast to the standard representation used by Haken in laser theory where $\alpha^{\dagger}=\alpha^{*}$, $v^{\dagger}=v^{*}$, and D is real, and

which does not in general provide a Fokker-Planck equation with a positive-definite diffusion matrix. Such generalized representations involving twice the usual number of dimensions were developed for the radiation field by Drummond and Gardiner.[32]

Following Haken, the equation of motion for P is derived and contains infinite-order derivatives. With N large one can use scaling arguments to ignore all but first- and second-order derivatives and to imply that the quantum noise terms (second-order derivatives) are small compared to the semiclassical (first-order derivative) terms. One can then transform the resulting Fokker-Planck equation with positive-definite diffusion into a stochastic differential equation.

The final equations derived (in a rotating frame where $\alpha \to \alpha e^{-i\omega_L t}$, $\alpha^\dagger \to \alpha^\dagger e^{i\omega_L t}$, $v \to v e^{-i\omega_L t}$, $v^\dagger \to v^\dagger e^{i\omega_L t}$) are

$$\begin{aligned}
\dot{\alpha} &= \varepsilon - \kappa(1+i\phi)\alpha + g v + \Gamma_\alpha(t) , \\
\dot{\alpha}^\dagger &= \varepsilon^* - \kappa(1-i\phi)\alpha^\dagger + g v^\dagger + \Gamma_{\alpha^\dagger}(t) , \\
\dot{v} &= -\gamma_\perp(1+i\Delta)v + g\alpha D + \Gamma_v(t) , \\
\dot{v}^\dagger &= -\gamma_\perp(1-i\Delta)v^\dagger + g\alpha^\dagger D + \Gamma_{v^\dagger}(t) , \\
\dot{D} &= -\gamma_\parallel(D+N) - 2g(v^\dagger\alpha + v\alpha^\dagger) + \Gamma_D(t) ,
\end{aligned} \tag{3a}$$

where

$$\phi = (\omega_c - \omega_L)/\kappa \quad \text{and} \quad \Delta = (\omega_0 - \omega_L)/\gamma_\perp .$$

The $\Gamma(t)$ are δ-correlated noise functions with zero mean. They describe the quantum fluctuations present and arise from the second-order derivatives (the diffusion matrix) of the Fokker-Planck equation. If these terms are ignored, one obtains the semiclassical equations of motion. The nonzero correlations of the quantum noise terms Γ are

$$\begin{aligned}
\langle \Gamma_\alpha(t)\Gamma_{\alpha^\dagger}(t')\rangle &= 2\kappa n_{\rm th}\delta(t-t') , \\
\langle \Gamma_v(t)\Gamma_v(t')\rangle &= \langle 2g\alpha v\rangle\delta(t-t') , \\
\langle \Gamma_{v^\dagger}(t)\Gamma_{v^\dagger}(t')\rangle &= \langle 2g\alpha^\dagger v^\dagger\rangle\delta(t-t') , \\
\langle \Gamma_D(t)\Gamma_D(t')\rangle &= \langle [2\gamma_\parallel(D+N) - 4g(v^\dagger\alpha + v\alpha^\dagger)]\rangle\delta(t-t') , \\
\langle \Gamma_v(t)\Gamma_{v^\dagger}(t')\rangle &= \langle (D+N)\gamma_p\rangle\delta(t-t') .
\end{aligned} \tag{3b}$$

$\gamma_\perp$ and $\gamma_\parallel$ are the transverse and longitudinal relaxation rates of the two-level atoms, respectively, while γ_p is the rate of collision-induced phase decay of the atoms ($\gamma_\perp = \gamma_p + \gamma_\parallel/2$). κ is the relaxation rate of the cavity and $n_{\rm th}$ is the mean number of thermal photons in the reservoir Γ_c

III. LINEARIZED THEORY OF FLUCTUATIONS

We are interested in the limit where the quantum fluctuation terms are small compared to the semiclassical or deterministic terms. In this limit of small fluctuations, one may solve for the transmitted spectrum by linearization of the equations about a stable semiclassical steady-state solution.

Ignoring quantum fluctuations altogether in the first instance, one may obtain the steady-state semiclassical or deterministic solutions α_0, v_0, D_0 ($\alpha_0^\dagger = \alpha_0^*$, $v_0^\dagger = v_0^*$)

$$v_0 = \frac{g\alpha_0 D_0}{\gamma_\perp(1+i\Delta)} , \quad D_0 = \frac{-N}{1+I/(1+\Delta^2)} , \tag{4a}$$

$$Y = I\left[\left[1+\frac{2C}{(1+\Delta^2+I)}\right]^2 + \left[\phi - \frac{2C\Delta}{(1+\Delta^2+I)}\right]^2\right]^{1/2} , \tag{4b}$$

$2C = g^2(N/\gamma_\perp\kappa)$ is the cavity cooperativity parameter and $I = |\alpha_0|^2/n_0$ and $Y = |\varepsilon|^2/\kappa^2 n_0$, where $n_0 = \gamma_\parallel\gamma_\perp/4g^2$ is the saturation intensity on resonance. The steady-state solution for the field (4b) is the optical bistability state equation in the mean-field theory approximation and has been well studied in previous works.[15,34]

Solutions are obtained in the limit of small fluctuations by linearizing Eq. (3) about the steady-state solutions α_0, v_0, D_0 of Eq. (4). Writing

$$\alpha = \alpha_0 + \delta\alpha, \quad v = v_0 + \delta v, \quad D = D_0 + \delta D , \tag{5}$$

we obtain the following equation, written in convenient matrix form, describing to first order the fluctuations in field and atomic variables:

$$\frac{d\delta\alpha}{dt} = -\underline{A}\,\delta\alpha + \underline{B}\,\varepsilon(t) , \tag{6a}$$

where

$$\delta\alpha = \begin{bmatrix} \delta\alpha \\ \delta\alpha^\dagger \\ \delta v \\ \delta v^\dagger \\ \delta D \end{bmatrix}, \quad \underline{A} = \begin{bmatrix} \kappa(1+i\phi) & 0 & -g & 0 & 0 \\ 0 & \kappa(1-i\phi) & 0 & -g & 0 \\ -gD_0 & 0 & \gamma_\perp(1+i\Delta) & 0 & -g\alpha_0 \\ 0 & -gD_0 & 0 & \gamma_\perp(1-i\Delta) & -g\alpha_0^\dagger \\ 2gv_0^\dagger & 2gv_0 & 2g\alpha_0^\dagger & 2g\alpha_0 & \gamma_\parallel \end{bmatrix}, \quad \mathbf{F}(t) = \underline{B}\,\varepsilon(t) = \begin{bmatrix} \Gamma_\alpha(t) \\ \Gamma_{\alpha^\dagger}(t) \\ \Gamma_v(t) \\ \Gamma_{v^\dagger}(t) \\ \Gamma_D(t) \end{bmatrix} .$$

Note $\langle \delta\boldsymbol{\alpha} \rangle = 0$. $\boldsymbol{\varepsilon}(t)$ is a δ-correlated noise vector with zero mean and such that

$$\langle \boldsymbol{\varepsilon}(t)\boldsymbol{\varepsilon}^T(t') \rangle = \underline{I}\delta(t-t') \ . \tag{6b}$$

The noise correlations are written

$$\langle \mathbf{F}(t)\mathbf{F}^T(t') \rangle = \underline{B}\langle \boldsymbol{\varepsilon}(t)\boldsymbol{\varepsilon}^T(t') \rangle \underline{B}^T = \underline{D}\delta(t-t') \ ,$$

$$\underline{D} = \begin{bmatrix} 0 & d_{\alpha\alpha^\dagger} & 0 & 0 & 0 \\ d_{\alpha\alpha^\dagger} & 0 & 0 & 0 & 0 \\ 0 & 0 & d_{vv} & d_{vv^\dagger} & 0 \\ 0 & 0 & d_{vv^\dagger} & d_{vv}^* & 0 \\ 0 & 0 & 0 & 0 & d_{DD} \end{bmatrix} = \underline{B}\,\underline{B}^T \ ,$$

$$d_{vv} = 2g\alpha_0 v_0, \quad d_{vv^\dagger} = (D_0+N)\gamma_p \ , \tag{6c}$$

$$d_{DD} = 2\gamma_\parallel (D_0+N) - 4g(v_0^*\alpha_0 + v_0\alpha_0^*) \ ,$$

$$d_{\alpha\alpha^\dagger} = 2\kappa n_{\text{th}} \ .$$

The diffusion array $\underline{D}$ is simply that of (3) but with α, v, D assuming their steady-state values (4).

The procedure of assuming small fluctuations about a steady-state deterministic solution is only consistent if the deterministic solution v_0, α_0, D_0 is stable. This is the case only if the eigenvalues of the matrix $\underline{A}$ have positive real parts.

IV. EXTERNAL INTENSITY AND SQUEEZING SPECTRA

Of particular interest to us is the field transmitted through the cavity port. We are interested in the intensity and squeezing spectra of the transmitted (output) field. We summarize here the results[35–40] enabling calculation of the spectra from the linearized equations (6).

The squeezing spectrum is defined as follows:

$$V(X_\theta,\omega) = \int_{-\infty}^{\infty} e^{i\omega\tau} \langle X_\theta(t+\tau), X_\theta(t) \rangle d\tau \ , \tag{7}$$

where

$$X_\theta(t) = a_{\text{out}}(t)e^{-i\theta} + a_{\text{out}}^\dagger(t)e^{i\theta}$$

is the quadrature phase amplitude of the transmitted (output) field. We use the notation $\langle X, Y \rangle = \langle XY \rangle - \langle X \rangle \langle Y \rangle$. We rewrite in terms of the boson operators:

$$V(X_\theta,\omega) = \int_{-\infty}^{\infty} e^{i\omega\tau} [\langle a_{\text{out}}(t+\tau), a_{\text{out}}^\dagger(t) \rangle + \langle a_{\text{out}}^\dagger(t+\tau), a_{\text{out}}(t) \rangle + \langle a_{\text{out}}(t+\tau), a_{\text{out}}(t) \rangle e^{-2i\theta} + \langle a_{\text{out}}^\dagger(t+\tau), a_{\text{out}}^\dagger(t) \rangle e^{2i\theta} \rangle] d\tau \ . \tag{8}$$

For a stationary or (stable) steady-state solution, the statistics will be independent of t, and we have $\langle a_{\text{out}}(t+\tau), a_{\text{out}}(t) \rangle = \langle a_{\text{out}}(\tau), a_{\text{out}} \rangle$. The relation between the output, input, and internal fields is given by the boundary condition at the cavity mirror which acts as an input/output port.[35,36] We take the optimal situation, discussed originally by Yurke,[38] of a single-ended cavity with transmission at only one mirror. The input field a_{in} in this case is the vacuum, and we assume the commutation relation

$$[a_{\text{in}}(t), a_{\text{in}}^\dagger(t')] = \delta(t-t') \ . \tag{9}$$

The theory developed by Collett and Gardiner[35,36] shows the following key results for the transmitted (or output) field:

$$\begin{aligned} &[a_{\text{out}}(t), a_{\text{out}}^\dagger(t')] = \delta(t-t'), \quad \langle a_{\text{out}}(\tau), a_{\text{out}} \rangle = 2\kappa \langle \delta\alpha(\tau), \delta\alpha \rangle \ , \\ &\langle a_{\text{out}}^\dagger(\tau), a_{\text{out}} \rangle = 2\kappa \langle \delta\alpha^\dagger(\tau), \delta\alpha \rangle \ . \end{aligned} \tag{10}$$

The output correlations relate directly to the c-number averages defined in the normally ordered P representation.[37] Thus the squeezing spectrum is

$$\begin{aligned} V(X_\theta,\omega) &= 1 + 2\kappa \int_{-\infty}^{\infty} e^{i\omega\tau} [\langle \delta\alpha^\dagger, \delta\alpha(\tau) \rangle + \langle \delta\alpha^\dagger(\tau), \delta\alpha \rangle + e^{-2i\theta} \langle \delta\alpha(t), \delta\alpha \rangle + e^{2i\theta} \langle \delta\alpha^\dagger(\tau), \delta\alpha \rangle] d\tau \\ &= 1 + 2\kappa [S_{12}(\omega) + S_{21}(\omega) + e^{-2i\theta} S_{11}(\omega) + e^{2i\theta} S_{22}(\omega)] \ , \end{aligned} \tag{11}$$

where we define the spectral matrix $\underline{S}(\omega) = [S_{ij}(\omega)]$ as the Fourier transform of the two-time correlation function $\langle \delta\boldsymbol{\alpha}(\tau), \delta\boldsymbol{\alpha}^T \rangle$

$$S_{ij}(\omega) = \int_{-\infty}^{\infty} e^{i\omega\tau} \langle \delta\alpha_i(\tau), \delta\alpha_j \rangle d\tau \ . \tag{12}$$

(The $\delta\alpha_j$ is the jth element of $\delta\boldsymbol{\alpha}$.) The solution for $\underline{S}(\omega)$ is readily derived[41–43] (see next section) for a stationary solution of the linear process (6). The result is

$$\underline{S}(\omega) = (\underline{A} - i\omega\underline{I})^{-1} \underline{D} (\underline{A}^T + i\omega\underline{I})^{-1} \ . \tag{13}$$

It is fruitful to discuss the result for the spectrum of squeezing of the output field in terms of the frequency components. ω_L is the reference output frequency (corresponding to, for example, the homodyne detector's local oscillator frequency). We may consider the quadrature phases $X_\theta(t)$ for the total output field at the detector as follows:

$$E_{\text{out}}(t)=(\lambda\omega_L)^{1/2}[a_{\text{out}}(t)e^{-i\omega_L t}+a^{\dagger}_{\text{out}}(t)e^{i\omega_L t}]$$
$$=(\lambda\omega_L)^{1/2}[X_\theta(t)\cos(\omega_L t-\theta)+X_{\theta+\pi/2}(t)\sin(\omega_L t-\theta)]\ , \tag{14}$$

where λ is a constant. We now consider a band of frequencies about ω_L. The field is then written

$$E_{\text{out}}(t)=\left[\frac{\lambda}{2\pi}\right]^{1/2}\int_{-\infty}^{\infty}\sqrt{\omega_L+\omega}\{a_{\text{out}}(\omega)e^{-i(\omega_L+\omega)t}+[a_{\text{out}}(\omega)]^{\dagger}e^{i(\omega_L+\omega)t}\}d\omega\ . \tag{15}$$

For practical purposes, at optical frequencies we may assume $(\omega_L+\omega)/\omega_L\simeq 1$, and we write

$$a_{\text{out}}(t)=\frac{1}{\sqrt{2\pi}}\int_{-\infty}^{\infty}a_{\text{out}}(\omega)e^{-i\omega t}d\omega,\quad a^{\dagger}_{\text{out}}(t)=\frac{1}{\sqrt{2\pi}}\int_{-\infty}^{\infty}[a_{\text{out}}(\omega)]^{\dagger}e^{i\omega t}d\omega\ . \tag{16}$$

The Fourier components are defined as the following Fourier transforms:

$$a_{\text{out}}(\omega)=\frac{1}{\sqrt{2\pi}}\int_{-\infty}^{\infty}a_{\text{out}}(t)e^{i\omega t}dt\ . \tag{17a}$$

We write the Fourier transform of $a^{\dagger}_{\text{out}}(t)$ as $a^{\dagger}_{\text{out}}(\omega)$, and note that $a^{\dagger}_{\text{out}}(\omega)=[a_{\text{out}}(-\omega)]^{\dagger}$. Thus

$$a^{\dagger}_{\text{out}}(\omega)=\frac{1}{\sqrt{2\pi}}\int_{-\infty}^{\infty}a^{\dagger}_{\text{out}}(t)e^{i\omega t}dt\ . \tag{17b}$$

We define similarly the Fourier components $a(\omega)$ of the internal field mode $a(t)$, and the Fourier amplitudes $\delta\alpha(\omega)$ and $\delta\alpha^{\dagger}(\omega)$ of the c-numbers $\delta\alpha(t)$ and $\delta\alpha^{\dagger}(t)$:

$$\delta\alpha(\omega)=\frac{1}{\sqrt{2\pi}}\int_{-\infty}^{\infty}\delta\alpha(t)e^{i\omega t}dt,\quad \delta\alpha^{\dagger}(\omega)=\frac{1}{\sqrt{2\pi}}\int_{-\infty}^{\infty}\delta\alpha^{\dagger}(t)e^{i\omega t}dt\ . \tag{17c}$$

The quadrature phase X_θ may be written in terms of its Fourier components as follows:

$$X_\theta(t)=\frac{1}{\sqrt{2\pi}}\int_{-\infty}^{\infty}\{a_{\text{out}}(\omega)e^{-i\theta}e^{-i\omega t}+[a_{\text{out}}(\omega)]^{\dagger}e^{i\theta}e^{i\omega t}\}d\omega$$
$$=\int_{-\infty}^{\infty}\{a_{\text{out}}(\omega)e^{-i\theta}+[a_{\text{out}}(-\omega)]^{\dagger}e^{i\theta}\}e^{-i\omega t}d\omega$$
$$=\int_{-\infty}^{\infty}X_\theta(\omega)e^{-i\omega t}d\omega\ , \tag{18}$$

where $X_\theta(\omega)=a_{\text{out}}(\omega)e^{-i\theta}+a^{\dagger}_{\text{out}}(\omega)e^{i\theta}$ is the Fourier transform of $X_\theta(t)$. We note that $X_\theta(\omega)$ is not Hermitian, in fact $[X_\theta(\omega)]^{\dagger}=X_\theta(-\omega)$. $X_\theta(t)$, however, is Hermitian, and we may rewrite

$$X_\theta(t)=\int_0^{\infty}\{X_\theta(\omega)e^{-i\omega t}+[X_\theta(-\omega)]^{\dagger}e^{i\omega t}\}d\omega\ . \tag{19}$$

The correlations of the frequency components for a stationary field are readily deduced using the properties of the δ function (we define $\tau=t-t'$),

$$\langle a_{\text{out}}(\omega),a_{\text{out}}(\omega')\rangle=\frac{1}{2\pi}\int_{-\infty}^{\infty}\int_{-\infty}^{\infty}e^{i\omega t}e^{i\omega' t'}\langle a_{\text{out}}(t),a_{\text{out}}(t')\rangle dt\,dt'$$
$$=\delta(\omega+\omega')2\kappa\int_{-\infty}^{\infty}e^{i\omega\tau}\langle\delta\alpha(\tau),\delta\alpha\rangle d\tau=\delta(\omega+\omega')2\kappa S_{11}(\omega)\ ,$$
$$\langle\alpha^{\dagger}_{\text{out}}(\omega),a_{\text{out}}(\omega')\rangle=\delta(\omega+\omega')2\kappa S_{21}(\omega)\ ,$$
$$\langle\alpha^{\dagger}_{\text{out}}(\omega),a^{\dagger}_{\text{out}}(\omega')\rangle=\delta(\omega+\omega')2\kappa S_{22}(\omega)\ ,$$
$$\langle a_{\text{out}}(\omega),a^{\dagger}_{\text{out}}(\omega')\rangle=\delta(\omega+\omega')+\langle a^{\dagger}_{\text{out}}(\omega'),a_{\text{out}}(\omega)\rangle=\delta(\omega+\omega')+\delta(\omega+\omega')2\kappa S_{12}(\omega)\ . \tag{20}$$

The commutation relation $[a_{\text{out}}(\omega),a^{\dagger}_{\text{out}}(\omega')]=\delta(\omega+\omega')$ is derivable from the output field commutation relation (10) (or vice versa).[34] It is straightforward to demonstrate $S_{11}(\omega)=S_{11}(-\omega)$, $S_{22}(\omega)=S_{22}(-\omega)$, and $S_{21}(\omega)=S_{12}(-\omega)$. We note that $a_{\text{out}}(\omega)$ will correlate only with $a_{\text{out}}(-\omega)$, i.e., the field at $\omega_L-\omega$ couples to the field at $\omega_L+\omega$. Also we note the transmitted field stationary intensity spectrum to be given by (to first order in

this linear theory)

$$\int_{-\infty}^{\infty} e^{i\omega\tau}\langle a_{\text{out}}^{\dagger}(\tau)a_{\text{out}}\rangle = 2\kappa\,|\,\alpha_0\,|^2\delta(\omega)+2\kappa S_{12}(\omega)\ . \quad (21)$$

The element $2\kappa S_{12}(\omega)$ is the (incoherent) intensity of the transmitted field at the frequency $\omega_L+\omega$, and $2\kappa S_{21}(\omega)$ is the intensity at $\omega_L-\omega$.

We find from the results (20),

$$\langle X_\theta(\omega),X_\theta(\omega')\rangle = \langle X_\theta(\omega),X_\theta\rangle\delta(\omega+\omega')\ , \quad (22)$$

where

$$\langle X_\theta(\omega),X_\theta\rangle = 1+2\kappa[S_{12}(\omega)+S_{21}(\omega) +e^{-2i\theta}S_{11}(\omega)+e^{2i\theta}S_{22}(\omega)]\ .$$

It is straightforward to show that the expression (7) for the squeezing spectrum may now be expressed

$$V(X_\theta,\omega)=\langle X_\theta(\omega),X_\theta\rangle \quad (23)$$

for a stationary state. The result is of course the same as (11).

For a coherent state, $V(X_\theta,\omega)=1$ and hence squeezing occurs for $V(X_\theta,\omega)<1$. Perfect squeezing corresponds to $V(X_\theta,\omega)=0$. One may optimize θ to give the minimum variance. We note that where $S_{11}(\omega)=[S_{22}(\omega)]^*$ and $S_{12}(\omega)=S_{21}(-\omega)$, the best squeezing is

$$V(X_\theta,\omega)=1+2\kappa[S_{12}(\omega)+S_{12}(-\omega)-2\,|\,S_{11}(\omega)\,|\,] \quad (24)$$

for

$$\cos\theta=-\frac{\mathrm{Re}S_{11}(\omega)}{|\,S_{11}(\omega)\,|},\quad \sin\theta=-\frac{\mathrm{Im}S_{11}(\omega)}{|\,S_{11}(\omega)\,|}\ .$$

V. THE SOLUTION FOR THE EXTERNAL FIELD SPECTRUM: WITHOUT ADIABATIC ELIMINATION

The solutions (11) and (13) enable us to calculate the external squeezing spectra $V(X_\theta,\omega)$ in the linear approximation. We have made no assumptions regarding the relative order of magnitudes of the atomic and cavity relaxation rates $\gamma_\perp$ and κ, respectively. Hence the technique used here enables investigation of the squeezing spectrum for a whole range of cavities. However, the direct matrix solution (13) for the spectrum matrix involves the tedious calculation of the inverse of 5×5 matrices.

A more convenient and illuminating way to gain insight into the various limits of relative decay rates $\gamma_\perp$ and κ and to enable a fully analytical solution is to consider the linear equation (6) in frequency space [cf. (17)]. We define

$$\delta\boldsymbol{\alpha}(\omega)=\frac{1}{\sqrt{2\pi}}\int_{-\infty}^{\infty}\delta\boldsymbol{\alpha}\,e^{i\omega t}dt\ ,$$
$$\mathbf{F}(\omega)=\underline{B}\,\boldsymbol{\varepsilon}(\omega)\ , \quad (25)$$
$$\boldsymbol{\varepsilon}(\omega)=\frac{1}{\sqrt{2\pi}}\int_{-\infty}^{\infty}\boldsymbol{\varepsilon}(t)e^{i\omega t}dt\ ,$$

where

$$\delta\boldsymbol{\alpha}^T(\omega)=(\delta\alpha(\omega),\ \delta\alpha^\dagger(\omega),\ \delta v(\omega),\ \delta v^\dagger(\omega),\ \delta D(\omega))$$

and

$$\mathbf{F}^T(\omega)=(\Gamma_\alpha(\omega),\ \Gamma_{\alpha^\dagger}(\omega),\ \Gamma_v(\omega),\ \Gamma_{v^\dagger}(\omega),\ \Gamma_D(\omega))\ .$$

The method developed here has a wider applicability. The approach is particularly useful for systems of large dimensionality, where eigenvalue solutions are not readily obtained. Equation (6a) in Fourier space becomes, for a stable stationary state

$$\mathbf{0}=(-\underline{A}-i\omega\underline{I})\delta\boldsymbol{\alpha}(\omega)+\mathbf{F}(\omega)\ . \quad (26a)$$

Rewriting explicitly, we have

$$\mathbf{0}=\begin{bmatrix} -\kappa[1+i\phi(\omega)] & 0 & g & 0 & 0\\ 0 & -\kappa[1-i\phi(-\omega)] & 0 & g & 0\\ gD_0 & 0 & -\gamma_\perp[1+i\Delta(\bar\omega)] & 0 & g\alpha_0\\ 0 & gD_0 & 0 & -\gamma_\perp[1-i\Delta(-\bar\omega)] & g\alpha_0^*\\ -2gv_0^* & -2gv_0 & -2g\alpha_0^* & -2g\alpha_0 & -\gamma_\parallel\left[1-\dfrac{i\omega}{\gamma_\parallel}\right] \end{bmatrix}\begin{bmatrix}\delta\alpha(\omega)\\ \delta\alpha^\dagger(\omega)\\ \delta v(\omega)\\ \delta v^\dagger(\omega)\\ \delta D(\omega)\end{bmatrix}+\begin{bmatrix}\Gamma_\alpha(\omega)\\ \Gamma_{\alpha^\dagger}(\omega)\\ \Gamma_v(\omega)\\ \Gamma_{v^\dagger}(\omega)\\ \Gamma_D(\omega)\end{bmatrix}, \quad (26b)$$

where we define $\phi(\omega)=\phi-\omega/\kappa$, $\Delta(\bar\omega)=\Delta-\bar\omega$, and $\bar\omega=\omega/\gamma_\perp$.

We notice the two scalings ω/κ and $\bar\omega=\omega/\gamma_\perp$ appearing. The cavity detuning $\phi=(\omega_c-\omega_L)/\kappa$ has been replaced by the true cavity detuning $\phi(\omega)=(\omega_c-\omega_L-\omega)/\kappa$ for the spectral amplitude $\delta\alpha(\omega)$ at frequency $\omega_L+\omega$. Similarly the atomic detuning $\Delta=(\omega_0-\omega_L)/\gamma_\perp$ becomes the true atomic detuning $\Delta(\bar\omega)=(\omega_0-\omega_L-\omega)/\gamma_\perp$ for the spectral amplitude at frequency $\omega_L+\omega$. The noise correlations in frequency space are, from the definitions (25) and using the result (6b), in matrix notation

$$\langle\boldsymbol{\varepsilon}(\omega)\boldsymbol{\varepsilon}^T(\omega')\rangle=\frac{1}{2\pi}\int_{-\infty}^{\infty}\int_{-\infty}^{\infty}e^{i\omega t}e^{i\omega' t}\langle\boldsymbol{\varepsilon}(t),\boldsymbol{\varepsilon}^T(t')\rangle dt\,dt' =\underline{I}\frac{1}{2\pi}\int_{-\infty}^{\infty}e^{i(\omega+\omega')t}dt=\underline{I}\delta(\omega+\omega') \quad (27a)$$

and

$$\langle\mathbf{F}(\omega)\mathbf{F}^T(\omega')\rangle=\underline{B}\langle\boldsymbol{\varepsilon}(\omega)\boldsymbol{\varepsilon}^T(\omega')\rangle\underline{B}^T =\underline{B}\,\underline{B}^T\delta(\omega+\omega')=\underline{D}\delta(\omega+\omega')\ .$$

Thus explicitly the nonzero noise correlations in frequency space are

$$\langle \Gamma_\alpha(\omega)\Gamma_{\alpha^\dagger}(\omega')\rangle = \delta(\omega+\omega')2\kappa n_{\rm th} ,$$
$$\langle \Gamma_v(\omega)\Gamma_v(\omega')\rangle = \delta(\omega+\omega')2g\alpha_0 v_0 ,$$
$$\langle \Gamma_{v^\dagger}(\omega)\Gamma_{v^\dagger}(\omega')\rangle = \delta(\omega+\omega')2g\alpha_0^* v_0^* , \tag{27b}$$
$$\langle \Gamma_D(\omega)\Gamma_D(\omega')\rangle = \delta(\omega+\omega') \times[2\gamma_\parallel(D_0+N)-4g(v_0^*\alpha_0+v_0\alpha_0^*)] ,$$
$$\langle \Gamma_v(\omega)\Gamma_{v^\dagger}(\omega')\rangle = \delta(\omega+\omega')(D_0+N)\gamma_p .$$

We now solve the nonadiabatically eliminated equations (26b) analytically in stepwise fashion. Only the field spectral correlations $[S_{22}(\omega),S_{12}(\omega),S_{21}(\omega)$ given by (11)] are of final interest to us. We therefore consider the last three lines of the matrix equation (26b) and eliminate $\delta D(\omega)$, to express the polarization $\delta v(\omega)$ in terms of the field alone. We point out that this is the same algebraic procedure as that usually taken where one adiabatically eliminates the atoms ($\gamma_\perp,\gamma_\parallel \gg \kappa$). The latter situation corresponds to $\bar\omega=0$. We make this comparison more carefully in Sec. VI. The result is

$$g\delta v(\omega) = -\kappa\gamma(\bar\omega)\delta\alpha(\omega) - \kappa b(\bar\omega)\delta\alpha^\dagger(\omega) + F_v(\omega) ,$$
$$g\delta v^\dagger(\omega) = -\kappa\gamma^*(-\bar\omega)\delta\alpha^\dagger(\omega) - \kappa b^*(-\bar\omega)\delta\alpha(\omega) + F_{v^\dagger}(\omega) , \tag{28a}$$

where

$$\gamma(\bar\omega)=\gamma_R(\bar\omega)+i\gamma_I(\bar\omega)=\frac{2C}{\Pi(0)}[1+i\Delta(\bar\omega)]\left[1-\frac{I}{2(1-i\Delta)\Pi(\bar\omega)}-\frac{I}{2[1+i\Delta(\bar\omega)]\Pi(\bar\omega)}\right] ,$$
$$b(\bar\omega)=\frac{-2C}{\Pi(0)}\frac{I}{2[1+i\Delta(\bar\omega)]\Pi(\bar\omega)}\left[\frac{1}{1+i\Delta}+\frac{1}{1-i\Delta(-\bar\omega)}\right] ,$$
$$\Pi(\bar\omega)=1-\frac{i\bar\omega}{2f}+\frac{I}{2[1+i\Delta(\bar\omega)]}+\frac{I}{2[1-i\Delta(-\bar\omega)]} ,$$

where $f=\gamma_\parallel/2\gamma_\perp$. We denote the real and imaginary parts of $\gamma(\bar\omega)$ by $\gamma_R(\bar\omega)$ and $\gamma_1(\bar\omega)$, respectively.

The stochastic term is

$$F_v(\omega)=\frac{g\Gamma_v(\omega)}{\gamma_\perp[1+i\Delta(\bar\omega)]}\left[1-\frac{I}{2\Pi(\bar\omega)[1+i\Delta(\bar\omega)]}\right]+\frac{g^2\alpha_0\Gamma_D(\omega)}{\gamma_\parallel\gamma_\perp[1+i\Delta(\bar\omega)]\Pi(\bar\omega)}-\frac{2g^3\alpha_0^2\Gamma_{v^\dagger}(\omega)}{\gamma_\parallel\gamma_\perp^2[1+i\Delta(\bar\omega)][1-i\Delta(-\bar\omega)]\Pi(\bar\omega)} ,$$
$$F_{v^\dagger}(\omega)=\frac{g\Gamma_{v^\dagger}(\omega)}{\gamma_\perp[1-i\Delta(-\bar\omega)]}\left[1-\frac{I}{2\Pi(\bar\omega)[1-i\Delta(-\bar\omega)]}\right]+\frac{g^2\alpha_0^*\Gamma_D(\omega)}{\gamma_\parallel\gamma_\perp[1-i\Delta(-\bar\omega)]\Pi(\bar\omega)}-\frac{2g^3\alpha_0^{*2}\Gamma_v(\omega)}{\gamma_\parallel\gamma_\perp^2[1+i\Delta(\bar\omega)]\Pi(\bar\omega)[1-i\Delta(-\bar\omega)]} . \tag{28b}$$

The correlations are

$$\langle F_v(\omega)F_v(\omega')\rangle = \kappa d(\bar\omega)\delta(\omega+\omega') ,$$
$$\langle F_{v^\dagger}(\omega)F_{v^\dagger}(\omega')\rangle = \kappa d^*(\bar\omega)\delta(\omega+\omega') ,$$
$$\langle F_v(\omega)F_{v^\dagger}(\omega')\rangle = \kappa\Lambda(\bar\omega)\delta(\omega+\omega') , \tag{28c}$$

$$d(\bar\omega)=-\frac{2CIf\left[1-\frac{I}{2\Pi(\bar\omega)[1+i\Delta(\bar\omega)]}\right]\left[1-\frac{I}{2\Pi(-\bar\omega)[1+i\Delta(-\bar\omega)]}\right]}{\Pi(0)(1+i\Delta)[1+i\Delta(\bar\omega)][1+i\Delta(-\bar\omega)]}$$
$$-\frac{2CI^2(1-f)}{2\Pi(0)(1+\Delta^2)}\frac{\left[1-\frac{I}{2\Pi(\bar\omega)[1+i\Delta(\bar\omega)]}\right]}{[1+i\Delta(\bar\omega)][1+i\Delta(-\bar\omega)][1-i\Delta(\bar\omega)]\Pi(-\bar\omega)}$$
$$-\frac{2CI^2(1-f)}{2\Pi(0)(1+\Delta^2)}\frac{\left[1-\frac{I}{2\Pi(-\bar\omega)[1+i\Delta(-\bar\omega)]}\right]}{[1+i\Delta(-\bar\omega)][1+i\Delta(\bar\omega)][1-i\Delta(-\bar\omega)]\Pi(\bar\omega)}$$
$$+\frac{2CI^2}{\Pi(0)(1+\Delta^2)|\Pi(\bar\omega)|^2[1+i\Delta(\bar\omega)][1+i\Delta(-\bar\omega)]}-\frac{2CI^3f}{4\Pi(0)(1-i\Delta)|\Pi(\bar\omega)|^2|1+i\Delta(\bar\omega)|^2|1+i\Delta(-\bar\omega)|^2} ,$$

$$\Lambda(\bar\omega)=\frac{2C(1-f)I\left|1-\frac{I}{2\Pi(\bar\omega)[1+i\Delta(\bar\omega)]}\right|^2}{\Pi(0)(1+\Delta^2)|1+i\Delta(\bar\omega)|^2}+\frac{2C(1-f)I^3}{4\Pi(0)(1+\Delta^2)|1+i\Delta(\bar\omega)|^2|1-i\Delta(-\bar\omega)|^2}$$
$$+\frac{2CI^2}{\Pi(0)(1+\Delta^2)|\Pi(\bar\omega)|^2|1+i\Delta(\bar\omega)|^2}+\mathrm{Re}\left[\frac{2CI^2f\left[1-\frac{I}{2\Pi(\bar\omega)[1+i\Delta(\bar\omega)]}\right]}{\Pi(0)\Pi^*(\bar\omega)|1+i\Delta(\bar\omega)|^2[1+i\Delta(-\bar\omega)](1+i\Delta)}\right] .$$

The solutions are functions of the following scaled parameters [cf. Eq. (4)]: $\bar{\omega}=\omega/\gamma_\perp$ the detuning of $\alpha(\omega)$ from the pump frequency in units of $\gamma_\perp$, Δ the atomic detuning in units of $\gamma_\perp$, the cooperativity parameter C, the scaled intracavity intensity I, and the collisional parameter f. In this paper, we will assume pure radiative damping ($f=1$). We note $d(\bar{\omega})=d(-\bar{\omega})$ and $\Lambda(\bar{\omega})=\Lambda(-\bar{\omega})$. We have taken, for convenience, the steady-state solution α_0 to be real. The phase of α_0 relative to the external driving field ε is determined by the optical bistability equation (4b).

One substitutes the solution (28a) into the top two lines of (26b) to derive the final equations for the field alone

$$0=-\kappa\begin{bmatrix} a(\bar{\omega})-i\omega/\kappa & b(\bar{\omega}) \\ b^*(-\bar{\omega}) & a^*(-\bar{\omega})-i\omega/\kappa \end{bmatrix}\begin{bmatrix} \delta\alpha(\omega) \\ \delta\alpha^\dagger(\omega) \end{bmatrix}+\begin{bmatrix} F_v(\omega)+\Gamma_\alpha(\omega) \\ F_v{}^\dagger(\omega)+\Gamma_\alpha{}^\dagger(\omega) \end{bmatrix},$$

$$a(\bar{\omega})=1+i\phi+\gamma_R(\bar{\omega})+i\gamma_I(\bar{\omega}) . \tag{29}$$

The equations are now of reduced dimension, being defined over *two-dimensional* complex phase space. These equations for the field spectrum, without adiabatic elimination, may be rewritten in the following matrix notation:

$$0=[-\underline{A}(\bar{\omega})+i\omega\underline{I}]\delta\boldsymbol{\alpha}_R(\omega)+\mathbf{F}_R(\omega) , \tag{30a}$$

where

$$\underline{A}(\bar{\omega})=\kappa\begin{bmatrix} a(\bar{\omega}) & b(\bar{\omega}) \\ b^*(-\bar{\omega}) & a^*(-\bar{\omega}) \end{bmatrix},\quad \delta\boldsymbol{\alpha}_R(\omega)=\begin{bmatrix} \delta\alpha(\omega) \\ \delta\alpha^\dagger(\omega) \end{bmatrix},$$

$$\mathbf{F}_R(\omega)=\begin{bmatrix} F_v(\bar{\omega})+\Gamma_\alpha(\omega) \\ F_v{}^\dagger(\bar{\omega})+\Gamma_\alpha{}^\dagger(\omega) \end{bmatrix}=\underline{B}(\bar{\omega})\boldsymbol{\varepsilon}(\omega) .$$

In this paper we assume negligible thermal noise ($n_{\rm th}=0$). The noise correlations are determined by the result (28c). On comparison with the original equation (26a), the reduced equation contains drift and diffusion parts now dependent on frequency, and we have introduced formally the notation $\underline{A}(\bar{\omega})$ and $\underline{B}(\bar{\omega})$. A frequency-dependent diffusion matrix $\underline{D}(\bar{\omega})$ is defined as follows:

$$\langle\mathbf{F}_R(\omega)\mathbf{F}_R^T(\omega')\rangle=\underline{B}(\bar{\omega})\langle\boldsymbol{\varepsilon}(\omega)\boldsymbol{\varepsilon}^T(\omega')\rangle\underline{B}^T(\bar{\omega}')=\underline{B}(\bar{\omega})\underline{B}^T(\bar{\omega}')\delta(\omega+\omega')=\underline{D}(\bar{\omega})\delta(\omega+\omega') . \tag{30b}$$

Thus $\underline{D}(\bar{\omega})=\underline{B}(\bar{\omega})B^T(-\bar{\omega})$, and the result (28c) gives us

$$\underline{D}(\bar{\omega})=\kappa\begin{bmatrix} d(\bar{\omega}) & \bar{\Gamma}(\bar{\omega}) \\ \bar{\Gamma}(\bar{\omega}) & d^*(\bar{\omega}) \end{bmatrix},\quad \bar{\Gamma}(\bar{\omega})=\Lambda(\bar{\omega})+2\kappa n_{\rm th} .$$

The solution for $\delta\boldsymbol{\alpha}_R(\omega)$ is readily expressed in matrix form

$$\delta\boldsymbol{\alpha}_R(\omega)=[\underline{A}(\bar{\omega})-i\omega\underline{I}]^{-1}\mathbf{F}_R(\omega) . \tag{31}$$

Thus the frequency correlations for the field are

$$\begin{aligned}\langle\delta\boldsymbol{\alpha}_R(\omega),\delta\boldsymbol{\alpha}_R^T(\omega')\rangle&=[\underline{A}(\bar{\omega})-i\omega\underline{I}]^{-1}\langle\mathbf{F}_R(\omega)\mathbf{F}_R(\omega')\rangle[\underline{A}^T(\bar{\omega}')-i\omega'\underline{I}]^{-1}\\&=[\underline{A}(\bar{\omega})-i\omega\underline{I}]^{-1}\underline{D}(\bar{\omega})[\underline{A}^T(\bar{\omega}')-i\omega'\underline{I}]^{-1}\delta(\omega+\omega') .\end{aligned} \tag{32}$$

The explicit matrix solution for the field spectrum defined in Eq. (12) of Sec. IV is now apparent. We define $\delta\boldsymbol{\alpha}_R^T(t)=(\delta\alpha(t),\delta\alpha^\dagger(t))$ and use the definition (25), the result (32), and the properties of the δ function

$$\begin{aligned}\underline{S}(\omega)&=\int_{-\infty}^{\infty}e^{i\omega\tau}\langle\delta\boldsymbol{\alpha}_R(\tau),\delta\boldsymbol{\alpha}_R^T\rangle d\tau\\&=\frac{1}{2\pi}\int_{-\infty}^{\infty}e^{i\omega\tau}d\tau\int_{-\infty}^{\infty}\int_{-\infty}^{\infty}e^{i\omega'(t+\tau)}e^{i\omega''t}\langle\delta\boldsymbol{\alpha}_R(\omega'),\delta\boldsymbol{\alpha}_R^T(\omega'')\rangle d\omega'\,d\omega''\\&=\frac{1}{2\pi}\int_{-\infty}^{\infty}\int_{-\infty}^{\infty}e^{i(\omega+\omega')\tau}[\underline{A}(\bar{\omega}')-i\omega'\underline{I}]^{-1}\underline{D}(\bar{\omega}')[A^T(-\bar{\omega}')+i\omega'\underline{I}]^{-1}d\tau\,d\omega'\\&=\int_{-\infty}^{\infty}\delta(\omega+\omega')[\underline{A}(\bar{\omega}')-i\omega'\underline{I}]^{-1}\underline{D}(\bar{\omega}')[\underline{A}^T(-\bar{\omega}')+i\omega'\underline{I}]^{-1}d\omega'\\&=[\underline{A}(\bar{\omega})-i\omega\underline{I}]^{-1}\underline{D}(\bar{\omega})[\underline{A}^T(-\bar{\omega})+i\omega\underline{I}]^{-1} .\end{aligned} \tag{33a}$$

The steps outlined in (33a), relating the spectrum $\underline{S}(\omega)$ directly to the frequency correlations $\langle\delta\boldsymbol{\alpha}(\omega),\delta\boldsymbol{\alpha}^T(\omega')\rangle$, are known to hold true in general for a stationary field and have been presented only for completeness.

The solution (33) for the field without adiabatic elimination is defined in terms of 2×2 matrices and is now readily ex-

pressed analytically. The solution has the same form as that derived by Drummond and Walls[15] for a high-Q cavity, but with the drift and diffusion matrices $\underline{A}$ and $\underline{D}$ becoming *frequency dependent.* The solution has the normalized form

$$\kappa \underline{S}(\omega)=\left[\frac{\underline{A}(\bar{\omega})}{\kappa}-\frac{i\omega \underline{I}}{\kappa}\right]^{-1}\frac{\underline{D}(\bar{\omega})}{\kappa}\left[\frac{\underline{A}^{T}(-\bar{\omega})}{\kappa}+\frac{i\omega \underline{I}}{\kappa}\right]^{-1} \tag{33b}$$

from which the adiabatic limits of high-Q ($\gamma_\perp \gg \kappa$) and low-Q ($\gamma_\perp \ll \kappa$) cavities are readily deduced. The high-Q solution has drift and diffusion matrices at zero frequency ($\bar{\omega}=\omega/\gamma_\perp=0$). The low-$Q$ solution has $i\omega \underline{I}/\kappa$ going to zero. The explicit result for the full solution is [$S_{22}(\omega)=S_{11}^{*}(\omega)$ and $S_{12}(\omega)=S_{21}(-\omega)$]

$$\begin{aligned}\kappa S_{11}(\omega)=&\frac{1}{|P(-i\omega)|^2}\{d(\bar{\omega})[a^{*}(\bar{\omega})a^{*}(-\bar{\omega})+q^2\bar{\omega}^2]+d^{*}(\bar{\omega})b(\bar{\omega})b(-\bar{\omega})-\bar{\Gamma}(\bar{\omega})[b(\bar{\omega})a^{*}(\bar{\omega})+b(-\bar{\omega})a^{*}(-\bar{\omega})]\\&-iq\bar{\omega}\,\bar{\Gamma}(\bar{\omega})[b(\bar{\omega})-b(-\bar{\omega})]+iq\bar{\omega}\,d(\bar{\omega})[a^{*}(-\bar{\omega})-a^{*}(\bar{\omega})]\}\ ,\\ \kappa S_{12}(\omega)=&\frac{1}{|P(-i\omega)|^2}\{-d(\bar{\omega})b^{*}(\bar{\omega})a^{*}(-\bar{\omega})-d^{*}(\bar{\omega})b(\bar{\omega})a(-\bar{\omega})-iq\bar{\omega}\,\bar{\Gamma}(\omega)[a(-\bar{\omega})-a^{*}(-\bar{\omega})]\\&+iq\bar{\omega}[d(\bar{\omega})b^{*}(\bar{\omega})-d^{*}(\bar{\omega})b(\bar{\omega})]+\bar{\Gamma}(\bar{\omega})[q^2\bar{\omega}^2+|a(-\bar{\omega})|^2+|b(\bar{\omega})|^2]\}\ ,\end{aligned} \tag{33c}$$

where

$$P(-i\omega)=[a(\bar{\omega})-iq\bar{\omega}][a^{*}(-\bar{\omega})-iq\bar{\omega}]-b(\bar{\omega})b^{*}(-\bar{\omega})$$

and

$$\bar{\omega}=\frac{\omega}{\gamma_\perp}\ \text{and}\ q=\frac{\gamma_\perp}{\kappa}\ .$$

The transmitted intensity and squeezing spectra κS_{12} and $V(X_\theta,\omega)$, respectively, are now readily calculated.

The solution (28) to the last three lines of the matrix equation (26b) has been published previously in a different context. The atomic expressions $\gamma_R(\bar{\omega}),\ldots,\Lambda(\bar{\omega})$ describe nondegenerate four-wave mixing between weak amplitudes shifted in frequency $\pm\omega$ from a pump field. The classical terms $\gamma_R(\bar{\omega})$, $\gamma_I(\bar{\omega})$, $b(\bar{\omega})$ were first derived by Fu and Sargent[44] and Boyd *et al.*[45] They have been discussed with reference to saturation spectroscopy,[16] four-wave mixing, and side-mode instabilities which occur in multimode cavities with atoms.[17] The quantum noise terms have since been derived by Sargent *et al.*[16] and Reid and Walls[19,20] and Ho, Kumar, and Shapiro[23] and used in recent studies[19–23] of quantum noise in nondegenerate four-wave mixing. The reader is referred to the references for more detailed discussions and plots of these atomic functions.

The functions $\gamma_R(\bar{\omega}),\ldots,\Lambda(\bar{\omega})$ describe the response of the *atoms* to the intracavity field. The function $\gamma_R(\bar{\omega})$ is the atomic absorption profile. One sees [Fig. 1(a)] a large absorption peak at the atomic resonance ω_0. There is a small gain peak at the frequency $2\omega_L-\omega_0$ due to the scattering process depicted in Fig. 1(b). The function $\gamma_I(\bar{\omega})$ is the dispersion profile, while $b(\bar{\omega})$ is the coupling (four-wave mixing) coefficient between weak fields at frequencies $+\omega$ and $-\omega$. Figure 1(c) plots $|b(\bar{\omega})|$ for large intensities saturating the atoms. There are three resonances, a small central peak at $\omega=0$ and two larger side peaks at the Rabi frequencies $\omega=\pm\gamma_\perp(\Delta^2+2I)^{1/2}$, indicating the Stark splitting of the atomic energy levels. The reason for particularly large coupling at the Rabi frequencies is the scattering depicting in Fig. 1(d).[45] There is an enhancement of a four-wave mixing process tending to emit a photon pair at frequencies $\omega_L\pm\Omega$, where Ω is the Rabi frequency. We will show later that this leads to significant squeezing at frequencies $\omega_L\pm\Omega$ in a single-mode low-Q cavity.[17] The atomic noise function $F_v(\omega)$ is the source of quantum fluctuations for the amplitude $\delta\alpha(\omega)$ at ω. The strength of correlation between fluctuations $F_v(\omega)$ and $F_v(-\omega)$ is given by $d(\bar{\omega})$. This phase-sensitive term is responsible for quantum phenomena such as squeezing and is noise generated by the processes which couple $\delta\alpha(\omega)$ and $\delta\alpha(-\omega)$, such as depicted in Fig. 1(d). Even if one could "turn off" all processes which couple $\delta\alpha(\omega)$ and $\delta\alpha(-\omega)$, the transmitted incoherent spectrum $2\kappa S_{12}(\omega)$ is not zero. There are photons reemitted due to a phase-insensitive fluorescence arising from spontaneous emissions. In a saturated resonant cavity [$\phi=\gamma_R(\bar{\omega})=\gamma_I(\bar{\omega})=0$], the transmitted intensity in the hypothetical absence of coupling [$b(\bar{\omega})=d(\bar{\omega})=0$] is $2\kappa S_{12}(\omega)=\Lambda(\bar{\omega})/[1+(\omega/\kappa)^2]$. The term $\Lambda(\bar{\omega})$ [which determines the correlation $\langle F_v^{\dagger}(\omega)F_v(\omega)\rangle$] may thus be thought of as the phase-sensitive fluorescence source term. It describes the noise generated at ω in the absence of all coupling between $\delta\alpha(\omega)$ and $\delta\alpha(-\omega)$. Figure 1(e) shows $\Lambda(\bar{\omega})$ for a pump intensity sufficient to saturate the atoms. The spectrum shows a clear central peak with Rabi side peaks at $\omega=\pm\gamma_\perp(2I+\Delta^2)^{1/2}$. This noise (which tends to detract from squeezing) is more significant at higher intensities and near the pump frequency ($\omega=0$). The functions $\gamma_R(\bar{\omega}),\ldots,\Lambda(\bar{\omega})$ describe the response of the atoms to the intracavity field and depend on the cavity variables (κ,ϕ,g) only in the sense of scaling I or C. The spectra

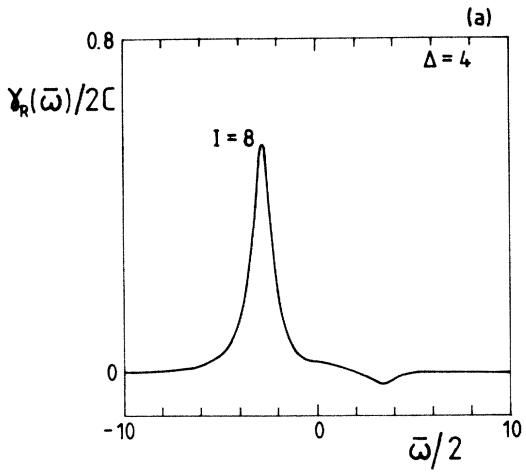

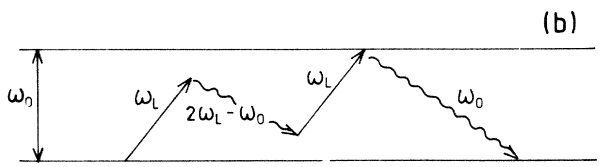

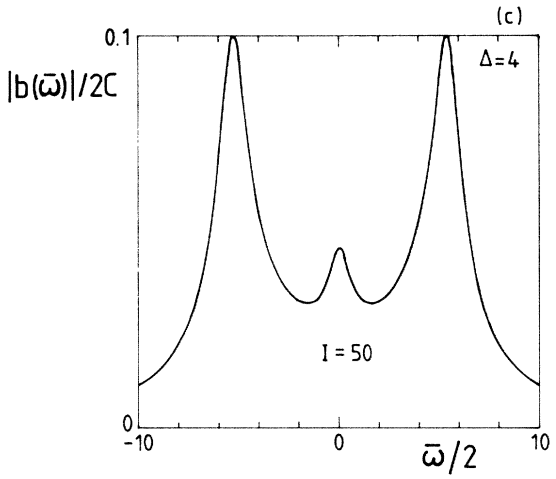

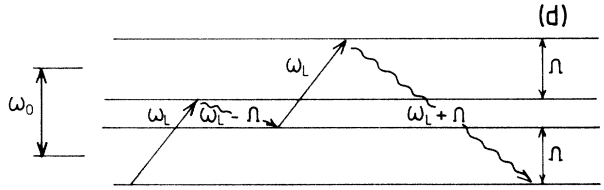

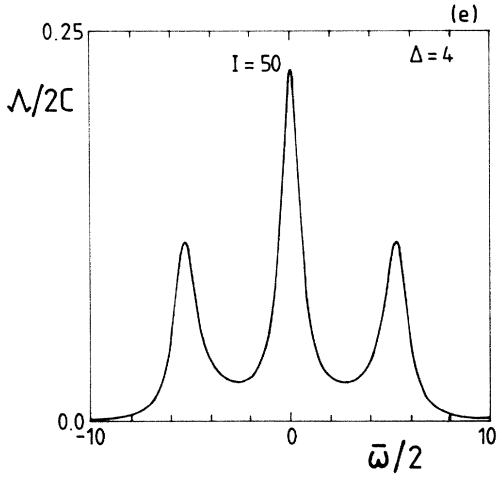

FIG. 1. (a) Plot of the atomic absorption profile $\gamma_R(\bar{\omega})$. $\Delta=4$, $I=8$. (b) Atomic scattering process for low intensities I. (c) Plot of the magnitude of the atomic coupling coefficient $|b(\bar{\omega})|$: $\Delta=4$, $I=50$. (d) Atomic scattering process at high intensities I. (e) The atomic fluorescence term $\Lambda(\bar{\omega})$ for a higher intensity $\Delta=4$, $I=50$, $f=1$.

$\gamma_R(\bar{\omega}), \ldots$ show atomic resonances like those of usual resonance fluorescence and do not reflect cavity resonances.

The full atom-cavity behavior is given by the final solution (33). The linearized solution (33) holds *only* for a stable stationary state, and it is thus necessary to check the stability of the steady-state solution (4). The eigenvalues λ of the drift matrix $-\underline{A}$ of Eqs. (6) are the roots of the following characteristic polynomial. Defining $\tilde{\lambda}=\lambda/\kappa$, $\bar{\lambda}=\lambda/\gamma_\perp$, the eigenvalues are given by

$$P(\lambda)=\tilde{\lambda}^2+\tilde{\lambda}[a(i\bar{\lambda})+a^*(-i\bar{\lambda}^*)]+a(i\bar{\lambda})a^*(-i\bar{\lambda}^*) -b(i\bar{\lambda})b^*(-i\bar{\lambda}^*)=0 . \quad (34a)$$

More directly, the characteristic polynomial is the fifth-order polynomial of the form

$$\tilde{\lambda}^5+a_5\tilde{\lambda}^4+a_4\tilde{\lambda}^3+a_3\tilde{\lambda}^2+a_2\tilde{\lambda}+a_1=0 , \quad (34b)$$

where the coefficients a_i are functions of q, f, I, ϕ, Δ, and C (see below). The stability criteria can be determined analytically using the Hurwitz criteria for stability. We obtain the following conditions for stability:

$$\begin{aligned} &(1)\ a_5>0 , \\ &(2)\ h_2=a_5a_4-a_3>0 , \\ &(3)\ h_3=h_2a_3+a_5(a_1-a_5a_2)>0 , \\ &(4)\ h_4=h_3a_2-h_2a_1a_4+a_1(a_1-a_5a_2)>0 , \\ &(5)\ a_1>0 , \end{aligned} \quad (35)$$

where

$$a_5=2+2q(1+f) ,$$

$$a_4=1+\phi^2+4q\left[1+f+\frac{C}{\Pi(0)}\right]+q^2[1+\Delta^2+2f(I+2)] ,$$

$$a_3=2q\left[(1+f)(1+\phi^2)+\frac{2C}{\Pi(0)}\right]+2q^2\left[4f+1+\Delta^2+2fI+\frac{2C}{\Pi(0)}\left[2f+1-\frac{fI}{1+\Delta^2}\right]\right]+q^3 2f(1+\Delta^2+I) ,$$

$$a_2=q^2\left[(1+\phi^2)(1+\Delta^2+4f+2fI)+\frac{4C}{\Pi(0)}(3-\phi\Delta)-\frac{4CfI(1+\phi\Delta)}{\Pi(0)(1+\Delta^2)}+\frac{4C^2}{\Pi(0)^2}\right]+4q^3\left[f(1+\Delta^2+I)+\frac{2C}{\Pi(0)}\right] ,$$

$$a_1=2fq^3\left[(1+\phi^2)(1+\Delta^2+I)+\frac{4C}{\Pi(0)}(1-\phi\Delta)+\left[\frac{2C}{\Pi(0)}\right]^2\left[1-\frac{I}{1+\Delta^2}\right]\right] .$$

The high-Q adiabatic limit ($\kappa\ll\gamma_\perp,\gamma_\parallel$) displays instability only for regimes where the slope $\partial Y/\partial I$ of the state equation (4b) is negative.[34] It is known that regimes of positive-slope instabilities can occur in single-mode bistability[46,47] for a more general choice of parameters. This is discussed by Lugiato *et al.*[47,48] Self-pulsing instability has been observed in experiments by Orozco *et al.*[49]

VI. THE HIGH-Q CAVITY ($\gamma_\perp/\kappa, \gamma_\parallel/\kappa\rightarrow\infty$)

There are two important limits of relative decay rates $\gamma_\perp$ and κ. Before discussing the full solution (33), we examine each of these limits. Perhaps the most commonly studied is the "high-Q" cavity,[12–15,18,31] where the cavity relaxation rate κ of the cavity mode is much smaller than the relaxation rates $\gamma_\perp,\gamma_\parallel$ for the atoms $\kappa\ll\gamma_\perp,\gamma_\parallel$. In this case the atomic variables may be adiabatically eliminated. This allows one to set $\delta\dot{v}=\delta\dot{v}^\dagger=\delta\dot{D}=0$ in Eq. (6) and then to eliminate δD to obtain an expression for δv and $\delta v^\dagger$ and hence for the field. We notice that the equations obtained in this high-Q limit are simply the nonadiabatic elimination equations (28) with $\bar{\omega}=0$. The final field equations, to be compared with (29), in frequency space are

$$0=-\kappa\begin{bmatrix} a(0)-i\omega/\kappa & b(0) \\ b^*(0) & a^*(0)-i\omega/\kappa \end{bmatrix}\begin{bmatrix}\delta\alpha(\omega)\\ \delta\alpha^\dagger(\omega)\end{bmatrix} +\begin{bmatrix}F_v(\omega)+\Gamma_\alpha(\omega)\\ F_v^\dagger(\omega)+\Gamma_\alpha^\dagger(\omega)\end{bmatrix} , \quad (36)$$

where

$$a(0)=1+i\phi+\gamma_R(0)+i\gamma_I(0)$$

and

$$\langle F_v(\omega)F_v(\omega')\rangle=\kappa d(0)\delta(\omega+\omega') ,$$

$$\langle F_v^\dagger(\omega)F_v(\omega')\rangle=\kappa\Lambda(0)\delta(\omega+\omega') .$$

The solution for the spectrum in this limit of adiabatic elimination of atomic variables is thus simply Eq. (33), but with ω put equal to zero in the atomic functions $a(\bar{\omega})$, $b(\bar{\omega})$, $d(\bar{\omega})$, and $\Lambda(\bar{\omega})$. We have

$$\underline{S}(\omega)=[\underline{A}(0)-i\omega\underline{I}]^{-1}\underline{D}(0)[\underline{A}^T(0)+i\omega\underline{I}]^{-1} . \quad (37)$$

Thus the explicit solution (33c) has $\bar{\omega}=0$, but is still a function of $\omega/\kappa=q\bar{\omega}$ which is finite. This is the solution obtained previously by Drummond and Walls.[15] We no-

tice by examining (33b) that the analytical solution (37) obtained by adiabatic elimination of atomic variables does indeed correspond to the full solution in the limit $\gamma_\perp/\kappa \to \infty$. The functions $\gamma(0)$, $b(0)$, $d(0)$, and $\Lambda(0)$ are

$$\gamma_R(0)=\frac{2C}{(1+\Delta^2)\left[1+\frac{I}{1+\Delta^2}\right]^2},$$

$$\gamma_I(0)=\frac{-2C\Delta}{(1+\Delta^2)\left[1+\frac{I}{1+\Delta^2}\right]^2},$$

$$b(0)=\frac{-2CI(1-i\Delta)}{(1+\Delta^2)^2\left[1+\frac{I}{1+\Delta^2}\right]^2}, \tag{38}$$

$$d(0)=\frac{-2CI}{(1+\Delta^2)^3\left[1+\frac{I}{1+\Delta^2}\right]^3}\times\left[(1-i\Delta)^3 f+i\Delta I(1-f)(1-i\Delta)+\frac{I^2}{2}\right],$$

$$\Lambda(0)=\frac{2CI}{(1+\Delta^2)^3\left[1+\frac{I}{1+\Delta^2}\right]^3}\times\left[(1+\Delta^2)(1-f)+I[2+\Delta^2(1-f)]+\frac{I^2}{2}\right].$$

The result (37) is perhaps not surprising. The photons emitted from the cavity are detected and the photocurrent spectrum analyzed. The zero-frequency component of the spectrum corresponds to a long detection counting time (relative to all other time scales of the system). In the adiabatic limit $\gamma_\perp,\gamma_\parallel \gg \kappa$, the time a photon is stored in the cavity before being emitted is determined solely by $(2\kappa)^{-1}$. All times are long compared to the atomic relaxation times, and hence only the zero-frequency component of the atomic profile is seen.

The solution $S_{12}(\omega)$ for the high-Q incoherent intensity spectrum has been derived and discussed previously[12–15] We revise these results in order to discuss the squeezing spectrum.

The characteristic polynomial $P(\lambda)$ given by (34) in the high-Q cavity limit is the quadratic

$$P(\lambda)=\tilde{\lambda}^2+\tilde{\lambda}[a(0)+a^*(0)]+|a(0)|^2-|b(0)|^2 \tag{39}$$

which has roots

$$\left.\begin{matrix}\tilde{\lambda}_1\\ \tilde{\lambda}_2\end{matrix}\right\}=-[1+\gamma_R(0)]\pm\{|b(0)|^2-[\phi+\gamma_I(0)]^2\}^{1/2}. \tag{40}$$

Thus the stability criteria, that the real part of both eigenvalues λ_1,λ_2 are negative, are

$$1+\gamma_R(0)>0,$$
$$|a(0)|^2=[1+\gamma_R(0)]^2+[\phi+\gamma_I(0)]^2>|b(0)|^2. \tag{41}$$

Clearly, the first condition is always satisfied. The optical bistability equation (4b) relates the intracavity intensity I to the external driving field. The equation has been studied extensively and criteria for bistability derived.[15,34]

The denominator in the expression (33c) for the spectrum can be factorized and rewritten as

$$P\left[-\frac{i\omega}{\kappa}\right]P\left[\frac{i\omega}{\kappa}\right]=\left[\left[\frac{\omega}{\kappa}+\mathrm{Im}\tilde{\lambda}_1\right]^2+(\mathrm{Re}\tilde{\lambda}_1)^2\right]\times\left[\left[\frac{\omega}{\kappa}+\mathrm{Im}\tilde{\lambda}_2\right]^2+(\mathrm{Re}\tilde{\lambda}_2)^2\right]. \tag{42}$$

The spectrum can thus be rewritten as into the sum of two Lorentzians. For the case where the imaginary part of the eigenvalues is nonzero we have

$$\left.\begin{matrix}\tilde{\lambda}_1\\ \tilde{\lambda}_2\end{matrix}\right\}=\mathrm{Re}\tilde{\lambda}\pm i\,\mathrm{Im}\tilde{\lambda}, \tag{43}$$

where

$$\mathrm{Re}\tilde{\lambda}=-[1+\gamma_R(0)],$$
$$\mathrm{Im}\tilde{\lambda}=\{[\phi+\gamma_I(0)]^2-|b(0)|^2\}^{1/2},$$

and the intensity spectrum may be written as

$$S_{12}(\omega)=\frac{-X_1\left[\frac{\omega}{\kappa}+\mathrm{Im}\tilde{\lambda}_I\right]+X_2}{\left[\frac{\omega}{\kappa}+\mathrm{Im}\tilde{\lambda}_1\right]^2+(\mathrm{Re}\tilde{\lambda}_1)^2}+\frac{X_1\left[\frac{\omega}{\kappa}-\mathrm{Im}\tilde{\lambda}_1\right]+X_3}{\left[\frac{\omega}{\kappa}-\mathrm{Im}\tilde{\lambda}_1\right]^2+(\mathrm{Re}\tilde{\lambda}_1)^2},$$

$$X_1=\left[\bar{\Gamma}(0)-\frac{B}{|\tilde{\lambda}|^2}\right]\Big/4\,\mathrm{Im}\tilde{\lambda},$$

$$X_2=\frac{\bar{\Gamma}(0)}{4}+\frac{B}{4|\tilde{\lambda}|^2}-\frac{A}{4\,\mathrm{Im}\tilde{\lambda}_1}, \tag{44}$$

$$X_3=\frac{\bar{\Gamma}(0)}{4}+\frac{B}{4|\tilde{\lambda}|^2}+\frac{A}{4\,\mathrm{Im}\tilde{\lambda}_1},$$

where

$$B=\bar{\Gamma}(0)[|a(0)|^2+|b(0)|^2]-d(0)b^*(0)a^*(0)-d^*(0)b(0)a(0),$$

$$A=\bar{\Gamma}(0)i[a^*(0)-a(0)]-i[b(0)d^*(0)-b^*(0)d(0)],$$

and

$$\bar{\Gamma}(0)=\Lambda(0)+2\kappa n_{\rm th} ,$$

and

$$|\tilde{\lambda}|^2=(\mathrm{Re}\tilde{\lambda})^2+(\mathrm{Im}\tilde{\lambda})^2 .$$

One sees two quasi-Lorentzian peaks symmetrically displaced from the pump frequency. The imaginary component of the eigenvalues determines the positions of the peaks, at least in the limit of small broadening ($\mathrm{Re}\tilde{\lambda}\to 0$). Various intensity and squeezing spectra are plotted in Fig. 2.

In the limit of small I ($I \ll \Delta^2$), corresponding to the stable lower branch, the eigenvalues are

$$\tilde{\lambda}_{1,2}=-[1+\gamma_R(0)]\pm i\,|\phi+\gamma_I(0)| \tag{45}$$

and the fluctuation term $\Lambda(0)$ is small compared to $d(0)$. The spectrum in the dispersive limit of large atomic detuning Δ becomes

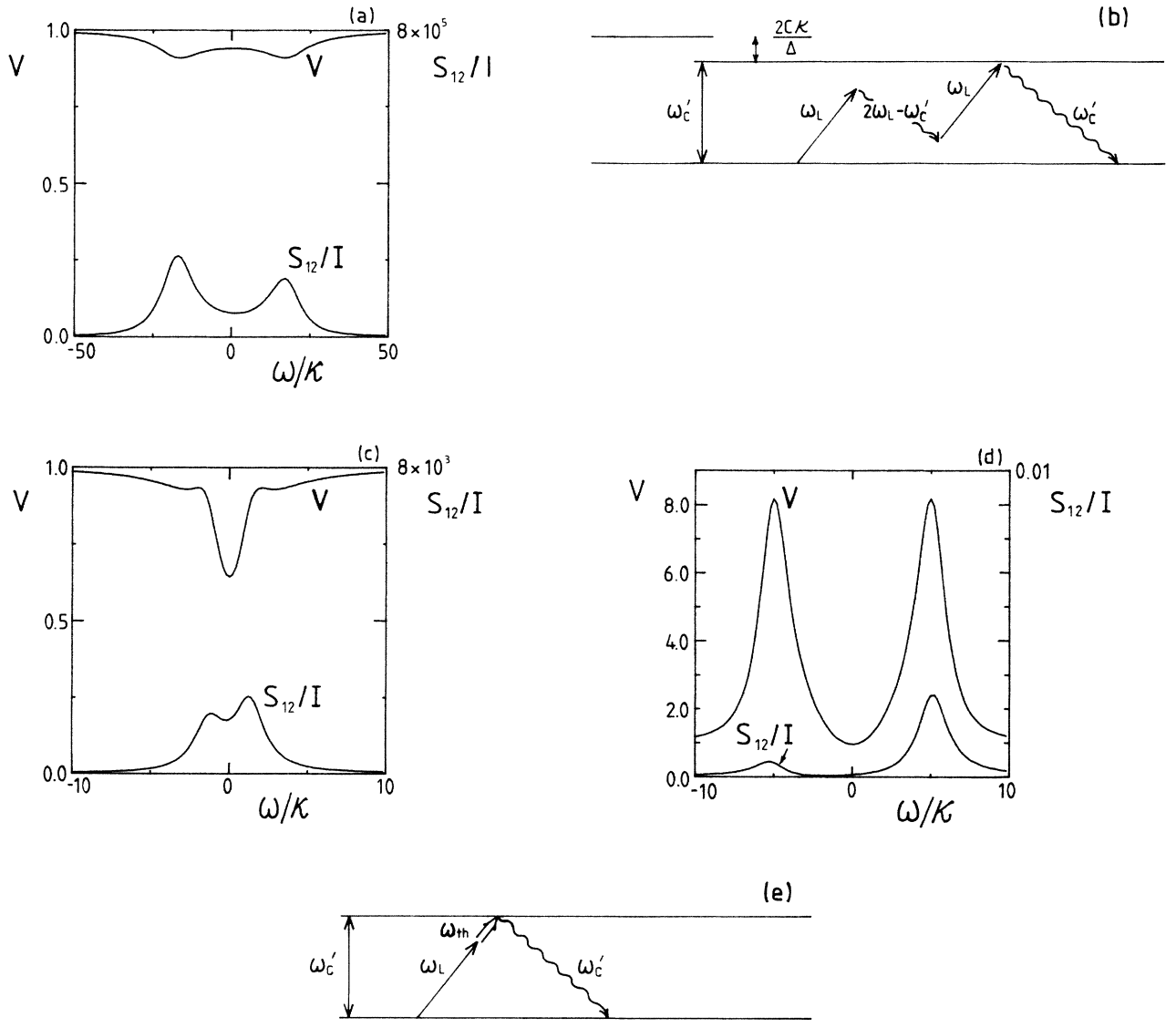

FIG. 2. The high-Q cavity limit. (a) Plots of the squeezing $[V(X_\theta,\omega)]$ and incoherent normalized intensity $[S_{12}(\omega)/I]$ spectra, $\Delta=100$, $C=1100$, $\phi=18$, $f=1$, $n_{\rm th}=0$, $I=100$ (corresponding to the lower branch of the optical bistability curve). (b) Inelastic scattering process giving rise to symmetric sidebands at ω_C' and $2\omega_L-\omega_C'$. For high detunings Δ and low intensities, $\omega_C'=\omega_C-2C\kappa/\Delta$. (c) $V(X_\theta,\omega)$ and $S_{12}(\omega)/I$. $\Delta=100$, $C=1100$, $\phi=18$, $f=1$, $n_{\rm th}=0$, and $I=2400$ (corresponding to nearer the turning point of the bistability curve). (d) $V(X_\theta,\omega)$ and $S_{12}(\omega)/I$. $\Delta=100$, $C=1100$, $\phi=18$, $f=1$, $n_{\rm th}=0$, and $I=4000$ (corresponding to the upper branch of the bistability curve). (e) Incoherent scattering process induced by broadband fluorescence (thermal-type) noise $\Lambda(0)$.

$$S_{12}(\omega)=\frac{-X_1\left[\frac{\omega}{\kappa}+\mathrm{Im}\tilde{\lambda}_1\right]-X_1\,\mathrm{Im}\tilde{\lambda}_1}{\left[\frac{\omega}{\kappa}+\mathrm{Im}\tilde{\lambda}_1\right]^2+(\mathrm{Re}\tilde{\lambda}_1)^2}+\frac{X_1\left[\frac{\omega}{\kappa}-\mathrm{Im}\tilde{\lambda}_1\right]-X_1\,\mathrm{Im}\tilde{\lambda}_1}{\left[\frac{\omega}{\kappa}-\mathrm{Im}\tilde{\lambda}_1\right]^2+(\mathrm{Re}\tilde{\lambda}_1)^2},$$

$$X_1=-\frac{|b(0)|^2[1+\gamma_R(0)]}{2|\lambda|^2\mathrm{Im}\tilde{\lambda}_1}. \tag{46}$$

The spectrum is symmetric about the input pump frequency ω_L (corresponding to $\omega=0$). The intensity and squeezing spectra [$S_{12}(\omega)$ and $V(X_\theta,\omega)$] corresponding to the lower branch are plotted in Fig. 2(a), for $\Delta=100$, $C=1100$, $\phi=18$.

The sidebands are explained by the inelastic scattering process depicted in Fig. 2(b).[50] The ω_c' represents the true cavity resonance including the refractive index of the medium [in this case for low I, we have approximately $\omega_c'=\omega_L+\kappa|\phi+\gamma_I(0)|$]. The scattering process enhances the frequencies ω_c' and $2\omega_L-\omega_c'$ equally, and one has a symmetric spectrum,[50] indicated by the limit (46). The squeezing spectrum shows enhancement of squeezing at the sidebands. This is not surprising, since squeezing has been long known to result from such coherent multiphoton scattering.[8]

There is spectral broadening[13] below threshold due to significant atomic absorption. This means that the doublet structure need not always be resolved. The absorption is a phase-insensitive process and reduces the squeezing possible. The effect of absorption increases with the cooperativity C value.[31]

Upon increasing I, the nonlinearity of the cavity increases and the squeezing improves. The cavity is closer to resonance with the external driving field and the side peaks move in together finally coalescing [Fig. 2(c)] as the bistable region is approached (and the imaginary component of the eigenvalues becomes zero). The spectra become single peaked about $\omega=0$ as the threshold region is approached. The squeezing is maximum at $\omega=0$ and improves as the turning points of the optical bistability equation are approached.[31]

Sufficiently high-I values correspond to the stable upper branch of the bistability curve. Moving along the upper branch (until $[\phi+\gamma_I(0)]^2>|b(0)|^2$), the spectrum [Fig. 2(d)] becomes double peaked again, corresponding to the appearance of imaginary eigenvalues. As the atoms saturate $\gamma_R(0),\gamma_I(0),b(0)\cdots\rightarrow 0$, there is linewidth narrowing to that of the cavity, and the doublet peaks approach $\omega_L\pm\kappa\phi$. For such high intensities approaching saturation ($I\rightarrow\Delta^2$), the fluorescence $\Lambda(0)$ at the pump frequency (corresponding to $\omega=0$) becomes significant.[31] One may study analytically the effect of this term on the spectrum by letting $\Lambda(0)$ dominate the coupling terms $d(0)$ and $b(0)$ in the solution (43). One obtains

$$S_{12}(\omega)=\frac{\Lambda(0)+2\kappa n_{\mathrm{th}}}{\left[\frac{\omega}{\kappa}-[\phi+\gamma_I(0)]\right]^2+[1+\gamma_R(0)]^2}. \tag{47}$$

The intensity spectrum is a single Lorentzian at the cavity resonance. Thus in general, above threshold the effect of the increasing fluorescence $\Lambda(0)$ is to make the spectrum asymmetric. This asymmetry is also enhanced by thermal noise n_{th} and, as described by Drummond and Walls[50] is due to scattering of the type depicted in Fig. 2(e). Unlike the coherent scattering process [Fig. 2(b)] discussed above this incoherent scattering will not enhance the squeezing, and one notes the variance in the quadrature phase increases at the side peaks of the high-Q spectrum above threshold.

In conclusion, for the high-Q cavity the atomic profiles (absorption $\gamma_R(\bar{\omega})$, coupling $b(\bar{\omega}),\ldots$) become broadband and show a flat spectrum compared to that of the cavity. The atomic profiles are seen at their zero-frequency ($\omega=0$) components (remembering as we are in a rotating frame, this corresponds to the pump frequency). Thus, for example, $b(\bar{\omega})$ and $\Lambda(\bar{\omega})$ for $I=50$ and $\Delta=4$ take the values indicated by $\omega=0$ in Figs. 1(c) and 1(d). As intensities increase towards saturation ($I\rightarrow\Delta^2$), there is enhancement of the phase-insensitive fluorescence $\Lambda(0)$ at zero frequency (corresponding to the center peak of the Stark triplet). While the Stark splitting provides a mechanism for significant enhancement of coupling $b(\bar{\omega})$ at the Rabi frequencies [Fig. 1(d)], no similar enhancement occurs at zero frequency. Thus in the high-Q cavity, $\Lambda(0)$ dominates at even moderate intensities, and the squeezing reduces. The phase insensitive fluorescence Λ is seen by the cavity as a broadband noise source and is analogous to a thermal noise term. Such noise tends to enhance the transmitted incoherent intensity at the cavity resonance frequency, resulting in an asymmetric intensity spectrum with increased noise at the cavity frequency.

In order to achieve best squeezing then, one requires intensities I in the low-saturation regime. Yet one needs sufficient nonlinearity $b(0)$. Consequently there is a window of optimal parameter range for I and C ($\Delta\ll I\ll\Delta^2$, $\Delta\ll 2C\ll\Delta^2$). This has been discussed previously.[31,51] The value of C used in Fig. 2 for $\Delta=100$ is about optimal, with the best squeezing achieved approaching the bistable regime. Lowering C, one requires greater intensities I to achieve a significant nonlinearity and thus squeezing is reduced well before the bistable region due to increased fluorescence $\Lambda(0)$. The spectra for the lower branch of lower-C cavities show greater asymmetry. We notice also the width of the spectral peaks to be reduced for lower C ($\gamma_R\rightarrow 0$). Increasing C, one increases phase insensitive absorption γ_R. Also to allow good squeezing, the cavity detuning ϕ is optimized to allow resonance of the nonlinear cavity with the pump field for the lowest intensity I possible.[31] High-atomic detunings are required.

We point out that the linearization procedure used is justified only where the order of fluctuations, as given by the intensity $\langle \delta\alpha^{\dagger}\delta\alpha \rangle$, are small compared to the steady-state deterministic intensity $|\alpha_0|^2 = I/n_0$. Thus we assume n_0 (or N) large. The figures reveal an increase in relative fluctuations $S_{12}(\omega)$ near the turning points of the optical bistability state equation. Our linearization procedure will break down at the turning point where fluctuations are large.

VII. THE LOW-Q CAVITY ($\gamma_\perp/\kappa, \gamma_\parallel/\kappa \to 0$)

The second limit of relative decay rates $\gamma_\perp$ and κ is the low-Q cavity[10,11,30] for which $\gamma_\perp, \gamma_\parallel \ll \kappa$. In this case the cavity-mode relaxation rate is much greater than the relaxation rate of the atoms. Hence the field variables may be adiabatically eliminated. This allows one to set $\delta\dot{\alpha} = \delta\dot{\alpha}^{\dagger} = 0$ in Eq. (6). The field equations become

$$\begin{aligned} 0 &= -\kappa(1+i\phi)\delta\alpha + g\,\delta v + \Gamma_\alpha(t) , \\ 0 &= -\kappa(1-i\phi)\delta\alpha^{\dagger} + g\,\delta v^{\dagger} + \Gamma_{\alpha^{\dagger}}(t) \end{aligned} \tag{48}$$

and for the atomic variables

$$\begin{aligned} \delta\dot{v} &= -\gamma_\perp(1+i\Delta)\delta v + gD_0\,\delta\alpha \\ &\quad + g\alpha_0\,\delta D + \Gamma_v(t) , \\ \delta\dot{v}^{\dagger} &= -\gamma_\perp(1-i\Delta)\delta v^{\dagger} + gD_0\,\delta\alpha^{\dagger} \\ &\quad + g\alpha_0^{*}\,\delta D + \Gamma_{v^{\dagger}}(t) , \\ \delta\dot{D} &= -\gamma_\parallel\delta D - 2gv_0^{*}\,\delta\alpha - 2gv_0\,\delta\alpha^{\dagger} \\ &\quad - 2g\alpha_0^{*}\,\delta v - 2g\alpha_0\,\delta v^{\dagger} + \Gamma_D(t) . \end{aligned} \tag{49}$$

The equations are rewritten in frequency space to obtain Eq. (26b) with $\phi(\omega) = \phi(0)$. The solution for the atomic $v(\omega)$ in terms of the field $\alpha(\omega)$ therefore takes the same form (28) as before. Thus the final equation for the field in frequency space is

$$\begin{aligned} 0 = -\kappa &\begin{bmatrix} a(\bar{\omega}) & -b(\bar{\omega}) \\ b^{*}(-\bar{\omega}) & a^{*}(-\bar{\omega}) \end{bmatrix} \begin{bmatrix} \delta\alpha(\omega) \\ \delta\alpha^{\dagger}(\omega) \end{bmatrix} \\ &+ \begin{bmatrix} F_v(\omega) + \Gamma_\alpha(\omega) \\ F_{v^{\dagger}}(\omega) + \Gamma_{\alpha^{\dagger}}(\omega) \end{bmatrix} , \end{aligned} \tag{50}$$

where

$$\begin{aligned} \langle F_v(\omega)F_v(\omega') \rangle &= \kappa d(\bar{\omega})\delta(\omega+\omega') , \\ \langle F_{v^{\dagger}}(\omega)F_{v^{\dagger}}(\omega') \rangle &= \kappa d^{*}(\bar{\omega})\delta(\omega+\omega') , \\ \langle F_{v^{\dagger}}(\omega)F_v(\omega') \rangle &= \kappa\Lambda(\bar{\omega})\delta(\omega+\omega') . \end{aligned}$$

The solution for the spectrum in the low-Q cavity adiabatic elimination limit is thus simply Eq. (33) but with ω/κ (i.e., $q\bar{\omega}$) put equal to zero and agrees with the limit $\kappa \to \infty$ of the full solution. The atomic functions $\gamma(\bar{\omega})$, $b(\bar{\omega})$, $d(\bar{\omega})$, and $\Lambda(\bar{\omega})$ retain the frequency dependence. We have

$$\underline{S}(\omega) = [\underline{A}(\bar{\omega})]^{-1}\underline{D}(\bar{\omega})[\underline{A}^{T}(\bar{\omega})]^{-1} . \tag{51}$$

The characteristic polynomial for the low-Q cavity limit is given by the cubic

$$\left[\bar{\lambda} = \frac{\lambda}{\gamma_\perp} \right] ,$$

$$\begin{aligned} &\bar{\lambda}^3 + a_3\bar{\lambda}^2 + a_2\bar{\lambda} + a_1 = 0 , \\ &a_3 = 2 + 2f + \frac{4C}{(1+\phi^2)\Pi(0)} , \\ &a_2 = 4f\left[1 + \frac{2C}{(1+\phi^2)\Pi(0)}\right] + \left[1 + \frac{2C}{\Pi(0)(1+\phi^2)}\right]^2 + \left[\Delta - \frac{2C\phi}{\Pi(0)(1+\phi^2)}\right]^2 - 2fI + \frac{4CfI(1+\Delta\phi)}{\Pi(0)(1+\Delta^2)(1+\phi^2)} , \\ &a_1 = 2f\left[\left[1 + \frac{2C}{(1+\phi^2)\Pi(0)}\right]^2 + \left[\Delta - \frac{2C\phi}{\Pi(0)(1+\phi^2)}\right]^2\right] \\ &\quad + 2fI\left[1 - \frac{2C(1+\Delta\phi)}{\Pi(0)(1+\Delta^2)(1+\phi^2)}\right]\left[1 + \frac{2C}{(1+\phi^2)\Pi(0)}\right] + 2fI\frac{2C(\Delta-\phi)}{\Pi(0)(1+\Delta^2)(1+\phi^2)}\left[\Delta - \frac{2C\phi}{\Pi(0)(1+\phi^2)}\right] . \end{aligned} \tag{52}$$

The Hurwitz stability criteria are

$$\begin{aligned} &(1)\ a_3 > 0 , \\ &(2)\ a_3a_2 - a_1 > 0 , \\ &(3)\ a_1 > 0 . \end{aligned} \tag{53}$$

The intensity spectrum $S_{12}(\omega)$ in this low-Q cavity limit has been derived and discussed previously.[11,30] We revise the results in order to discuss the squeezing spectra. Preliminary results were presented in an earlier work.[25] In principle, the spectrum can be decomposed into three quasi-Lorentzians, as determined by the three roots λ_i of the characteristic polynomial.

For small intensities $I \ll \Delta^2$ the eigenvalues become

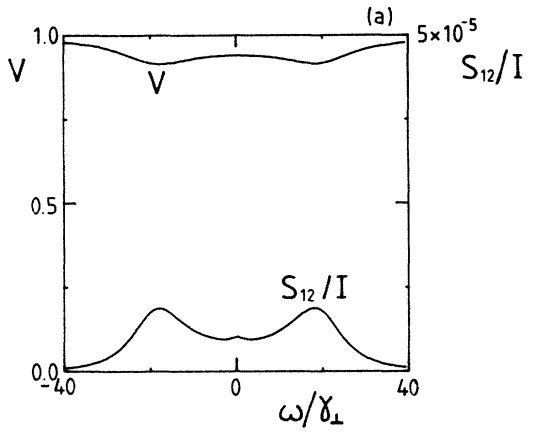

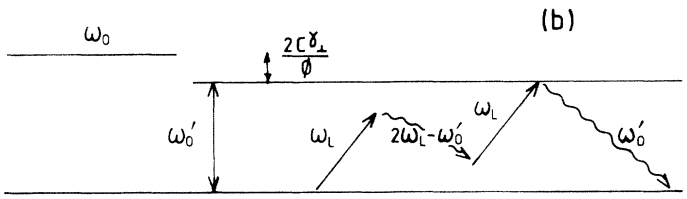

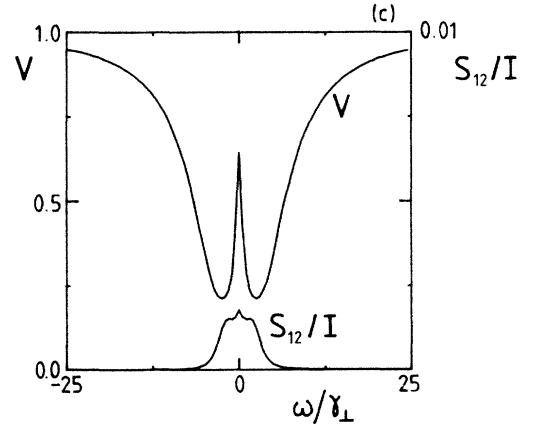

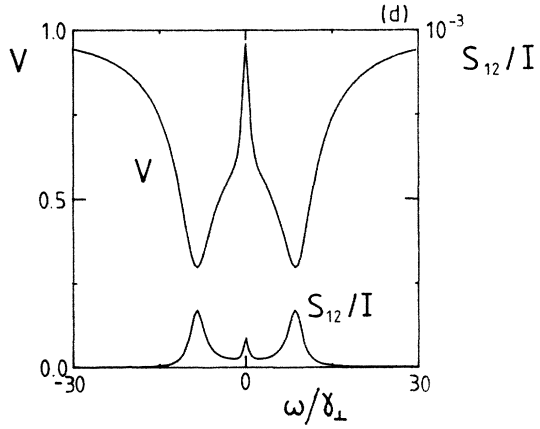

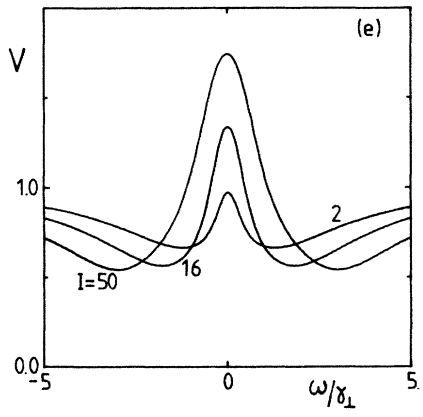

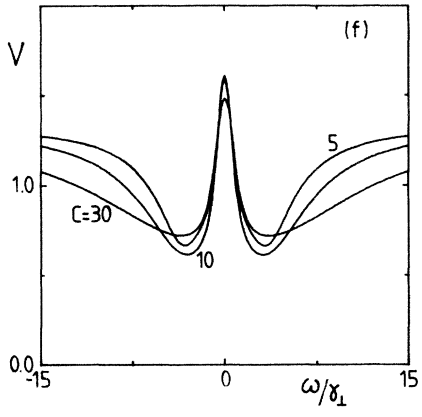

FIG. 3. The low-Q cavity limit. (a) Plots of the squeezing $[V(X_\theta,\omega)]$ and intensity $[S_{12}(\omega)/I]$ spectra. $\Delta=100$, $C=1100$, $\phi=18$, $f=1$, $n_{\rm th}=0$, and $I=100$. (b) Scattering process giving rise to sidebands at ω_0' and $2\omega_L-\omega_0'$. For high detunings ϕ and low intensities, we have approximately $\omega_0'=\omega_0-2C\gamma_\perp/\phi$. (c) $V(X_\theta,\omega)$ and $S_{12}(\omega)/I$. $\Delta=100$, $C=1100$, $\phi=18$, $f=1$, $n_{\rm th}=0$, and $I=2400$. (d) $V(X_\theta,\omega)$ and $S_{12}(\omega)/I$. $\Delta=100$, $C=1100$, $\phi=18$, $f=1$, $n_{\rm th}=0$, and $I=4000$. The phase angle θ for optimal squeezing at the sidepeaks is 0. (e) $V(X_\theta,\omega)$ for $\Delta=4$, $C=5$, $\phi=0$, $f=1$, $n_{\rm th}=0$. Significant squeezing is obtainable in the low-Q cavity limit even with very low atomic detunings Δ and C values. The mechanism for the enhancement in squeezing is depicted in Fig. 1(d). (f) $V(X_\theta,\omega)$ for $\Delta=8$, $\phi=0$, $f=1$, $n_{\rm th}=0$, and $I=64$.

$$\bar{\lambda}_{1,2}=1+\frac{2C}{1+\phi^2}\pm i\left[\Delta-\frac{\phi 2C}{1+\phi^2}\right],$$
$$\bar{\lambda}_3=\gamma_{\parallel}/\gamma_{\perp}\ . \tag{54}$$

The decomposition of the intensity spectrum $S_{12}(\omega)$ into the three corresponding Lorentzians in this low-intensity limit is given in Ref. 30. The component associated with the third eigenvalue vanishes, and the spectrum is a broadened doublet. Both the linewidth and the splitting of the doublet is modified by the cavity detuning ϕ. Figure 3(a) plots the intensity and squeezing spectrum corresponding to $I=100$, the lower branch of the optical bistability curve with $\Delta=100$, $C=1100$, and $\phi=18$. The sidebands are explained by the inelastic scattering process of the type depicted in Fig. 1(b), but replacing ω_0 with ω_0', the true atomic resonance incorporating the shift due to the cavity. The scattering depicted here [Fig. 3(b)] enhances both frequencies ω_0' and $2\omega_L-\omega_0'$ equally and the intensity spectrum is symmetric. The squeezing spectrum shows enhancement of squeezing at the sidebands due to the multiphoton process.

As the intensity I increases, the peak situated at $\omega=0$ appears and dominates as the turning point of the bistability equation is approached. The squeezing at the side bands improves with increasing intensity [Fig. 3(c)].

Sufficient I corresponds to the stable upper branch. Figure 3(d) plots the intensity and squeezing spectra corresponding to $I=4000$, a point on the upper branch. Here there are three peaks. As the bistable region is approached, the sidepeaks move in closer to the central peak. Far enough above the bistable region on the upper branch, the atoms saturate, and the spectrum tends to the usual triplet of one-atom fluorescence.[30] There is a significant central peak at $\omega=0$ and two sidepeaks located at the Rabi frequencies

$$\frac{\omega}{\gamma_{\perp}}=\pm\frac{\Omega}{\gamma_{\perp}}=\pm(\Delta^2+2I)^{1/2}\ .$$

At such intensities I saturating the atoms, there is a Stark splitting of the (dressed) energy levels of the two level atom as depicted in Fig. 1(d). The resonant inelastic scattering now involves absorption of two laser photons at frequency ω_L and emission of photons at the sideband frequencies $\omega_L\pm\Omega$. The squeezing is enhanced for these sidebands since they are generated via a two-photon process. The dressed atom also has energy levels separated by the laser frequency and thus the presence of the center peak at $\omega=0$, but we notice this central peak to correspond to increased noise (reduced squeezing). Unlike the sidepeak photons, the photons scattered at the pump frequency ($\omega=0$) are not scattered as part of a process resulting in the coherent emission of two photons.

We discuss also the phase angle 2θ at which maximum noise reduction (squeezing) is obtained. Consider the high-intensity situation depicted in Fig. 3(d). At $\omega=0$, the optimal angle is $2\theta=-104°$. As ω increases, the angle rotates until at the sidepeaks the phase angle is $\theta=0$. The fluctuations are reduced in the direction of the coherent amplitude α_0—we have something similar to photon antibunching. This is usual of situations on resonance with an atomic energy level, for example, absorptive bistability. The Stark splitting of energy levels in this case provides a mechanism [Fig. 1(d)] for strong amplitude squeezing (antibunching) for frequencies on resonance with an atomic transition.

We compare the spectrum of the low-Q cavity above threshold with the high-Q cavity result. For the high-Q cavity the bandwidth of the external field is narrow and located within the central atomic fluorescence peak. The phase-insensitive fluorescence $\Lambda(0)$ destroys the squeezing and causes asymmetry of the sideband intensities. The bandwidth of the low-Q cavity spectrum is not restricted by the field relaxation rate κ in this manner, and the frequency components move out to the sidepeaks of the atomic fluorescence where the coupling process Fig. 1(d) enhances squeezing.

The avoidance of the phase-insensitive fluorescence $\Lambda(0)$ in the low-Q cavity and the coupling possible at the sidepeaks for large intensities permits good squeezing to be obtained for a much wider range of cavity parameters Δ, C, ϕ, and I than is possible in the high-Q case.[25] Good squeezing is possible for low Δ, C, and I values [Figs. 3(e) and 3(f)]. We notice from (50) that the particular amplitude $\delta\alpha(\omega)$ will have atomic dispersion $\gamma_I(\bar{\omega})$, fluorescence $\Lambda(\bar{\omega})\cdots$. The effective detuning of $\delta\alpha(\omega)$ from the empty cavity, however, is ϕ (independent of frequency ω because of the relative cavity and atomic timescales). The $\gamma_I(\bar{\omega})$ is the change in the resonance frequency of the cavity due to the atoms, as seen at frequency ω [in absence of coupling $b(\omega)$]. In general the greater nonlinearity (hence squeezing) is achieved for $\phi+\gamma_I(\omega)\sim 0$. At low intensities, we have $\gamma_I\sim(-2C)/\Delta$ for low frequencies and $\phi\sim(2C)/\Delta$ is the optimum cavity detuning. At higher intensities γ_1 saturates (more readily than the coupling b), and the better nonlinearity (squeezing) is obtained for smaller cavity detunings, $\phi\rightarrow 0$ [Fig. 3(e)]. At the narrow resonance [Fig. 1(c)] corresponding to the Rabi frequency, the coupling is large, and good squeezing is obtained at the Rabi side peaks for a range of detunings ϕ. However, the smaller values of ϕ will correspond to broader sidepeaks and hence broader-band squeezing. Figure 3(f) demonstrates a variation in behavior with C. Lower-C cavities require greater intensities for sufficient coupling, which reduces squeezing at the center frequency, but considerable squeezing is obtainable at side peaks. Higher-C cavities ($2C>\Delta^2$) have large absorption γ_R at low and moderate intensities $I\leq\Delta^2$ and hence reduced squeezing. However at much higher intensities, the absorption saturates more quickly than the coupling, and good squeezing is possible at the sidepeaks.

We point out a connection between the linearized "low-Q limit" spectrum [$\underline{S}(\omega)$ of 33] and results predicted for intracavity (nondepleting) nondegenerate four-wave mixing.[19–22] In the latter situation, we have two cavity side modes separated in frequency $\pm\omega$ from the central (driven) resonant cavity mode. One may (providing there is stability) derive the transmitted spectrum [$\underline{S}(\omega,\bar{\omega})$, say] to describe the field at frequency $\omega+\bar{\omega}$

from the pump. If we happen to calculate the zero-frequency ($\bar{\omega}=0$) component of this spectrum, to obtain $\underline{S}(\omega,0)$, we recover the low-Q limit spectrum [$\underline{S}(\omega,0)=\underline{S}(\omega)$].[20] This is not surprising, since the intracavity side-mode field at ω has the same atomic profile as the single-mode frequency amplitude $\delta\alpha(\omega)$. The side modes, however, are independent modes [unlike the $\delta\alpha(\omega)$ of the single-mode cavity] and build up in a different manner. In particular, the stability properties of the two cases differ. The cavity side modes generally become unstable at the cavity-mode frequencies ω which correspond to the sidepeaks (and hence best squeezing) in the low-Q single-mode spectrum. This is because side modes at these frequencies see enhanced gain.[17]

VIII. THE GENERAL CAVITY

We discuss the general cavity with κ, $\gamma_\perp$, $\gamma_\parallel$ arbitrary. From (29), we see the field amplitude $\delta\alpha(\omega)$ to be given by

$$0=-\kappa[1+i\phi(\omega)+\gamma_R(\bar{\omega})+i\gamma_1(\bar{\omega})]\delta\alpha(\omega) +\kappa b(\bar{\omega})\delta\alpha^\dagger(\omega)+\bar{F}(\omega) \tag{55}$$

[and the corresponding equation for $\delta\alpha^\dagger(\omega)$], where

$$\phi(\omega)=\phi-\frac{\omega}{\kappa}=\phi-q\bar{\omega} ,$$
$$\langle\bar{F}(\omega)\bar{F}(\omega')\rangle=\kappa d(\bar{\omega})\delta(\omega+\omega') ,$$
$$\langle\bar{F}^\dagger(\omega)\bar{F}^\dagger(\omega')\rangle=\kappa d^*(\bar{\omega})\delta(\omega+\omega') ,$$
$$\langle\bar{F}(\omega)\bar{F}^\dagger(\omega')\rangle=\kappa\bar{\Gamma}(\bar{\omega})\delta(\omega+\omega') .$$

Thus the amplitude $\delta\alpha(\omega)$ at frequency ω sees the atomic functions [absorption $\gamma_R(\bar{\omega})$, coupling $b(\bar{\omega})\cdots$] at the relevant scaled frequency $\bar{\omega}=\omega/\gamma_\perp$. The amplitude $\delta\alpha(\omega)$ also sees the true cavity detuning $\phi(\omega)=\phi-\omega/\kappa$. The full solution for the spectrum is thus now a superposition of two frequency-dependent functions—that for the cavity and that for the atoms. Towards the low-Q cavity limit $q=\gamma_\perp/\kappa\to 0$, the cavity function broadens relative to the atomic functions, thus $\phi(\omega)\to\phi(0)$. Similarly, toward the high-Q cavity limit $\gamma_\perp/\kappa\to\infty$, the atomic variables take their long-time behavior and the atomic functions broaden relative to the cavity functions, thus

$$\gamma_R(\bar{\omega})\to\gamma_R(0)\cdots .$$

Before discussing the new features of a more general nonadiabatic cavity, it is important to note that the result for the spectrum at the central (or pump) frequency $\omega=0$ is unchanged with q. This point has been made by Savage and Walls[52] and is clear from the explicit solution (33) for the spectrum. The zero-frequency result corresponds to long counting times, greater than both the cavity and atomic relaxation times.

The characteristic polynomial for the general cavity is now a fifth-order polynomial. In the zero-intensity limit $\alpha_0\to 0$, the inversion decouples from the field and polarization variables in Eq. (6) (to give an eigenvalue $\lambda_1=-\gamma_\parallel$). The eigenvalues of the coupled field-polarization system are

$$\lambda_{2,3}=\mathrm{Re}\lambda_{2,3}+i\,\mathrm{Im}\lambda_{2,3} ,\quad \lambda_4=\lambda_2^* ,\quad \lambda_5=\lambda_3^* ,$$
$$\mathrm{Re}\lambda_{2,3}=-\frac{(\gamma_\perp+\kappa)}{2} \pm\tfrac{1}{2}[Z_R+(Z_R^2+Z_I^2)^{1/2}]^{1/2} ,$$
$$\mathrm{Im}\lambda_{2,3}=-\frac{(\gamma_\perp\Delta+\kappa\phi)}{2} \pm\tfrac{1}{2}[-Z_R+(Z_R^2+Z_I^2)^{1/2}]^{1/2} , \tag{56a}$$

where

$$2Z_R=(\gamma_\perp-\kappa)^2-4g^2N-(\gamma_\perp\Delta-\kappa\phi)^2 =(\gamma_\perp-\kappa)^2-4g^2N-(\omega_0-\omega_C)^2 ,$$
$$2Z_1=2(\gamma_\perp-\kappa)(\gamma_\perp\Delta-\kappa\phi) =2(\gamma_\perp-\kappa)(\omega_0-\omega_C) .$$

In the absorptive limit (where $\Delta=\phi=0$) there is the simplification

$$\lambda_{2,3}=\begin{cases} -\dfrac{(\gamma_\perp+\kappa)}{2}\pm\tfrac{1}{2}[(\gamma_\perp-\kappa)^2-4g^2N]^{1/2} , \\ \qquad \text{if } |\gamma_\perp-\kappa|>2g\sqrt{N} \\ -\dfrac{(\gamma_\perp+\kappa)}{2}\pm\dfrac{i}{2}[4g^2N-(\gamma_\perp-\kappa)^2]^{1/2}, \\ \qquad \text{if } |\gamma_\perp-\kappa|<2g\sqrt{N} . \end{cases} \tag{56b}$$

where the upper signs (+) in Eq. (56b) refer to λ_2 and the lower signs (−) to λ_3. This case of absorptive bistability was pointed out by Carmichael,[26] and we summarize results. For large κ ($q=\gamma_\perp/\kappa\to 0$, the low-$Q$ cavity limit) we may write the eigenvalues (provided $q,8Cq\ll 1$) as

$$\lambda_{2,3}=\lambda_{4,5}=-\frac{(\gamma_\perp+\kappa)}{2}\pm\frac{\kappa}{2}[1-q(1+4C)+O(q^2)] . \tag{57}$$

The eigenvalues are real. Thus the spectrum will be a superposition of Lorentzians centered at $\omega=0$. The Lorentzians corresponding to λ_3 and λ_5 have the broad cavity half-linewidth κ and are noneffectual. The eigenvalues λ_2, λ_4 become in this low-Q cavity limit

$$\lambda_2=\lambda_4=-\gamma_\perp(1+2C) ,$$

which agrees with the adiabatic elimination result (54). The high-Q limit of large $\gamma_\perp$ ($1/q \to 0$ and $(8C)/q \ll 1$) may be handled similarly to reveal

$$\lambda_{2,3}=\lambda_{4,5}=-\frac{(\gamma_\perp+\kappa)}{2} \pm\frac{\gamma_\perp}{2}\left[1-\frac{1}{q}(1+4C)+O(1/q^2)\right] . \quad (58)$$

Again the eigenvalues are real. The eigenvalues λ_1, λ_3, λ_5 now correspond to Lorentzians with the broad atomic linewidth and are noneffectual. The effective eigenvalues are λ_2, λ_4 as in the adiabatic limit (45).

Examining the absorptive solution (56b), it is apparent that for a range of intermediate q values the eigenvalues develop a nonzero imaginary component, the eigenvalues being[26]

$$\lambda_{2,3}=\lambda_{4,5}=-\frac{(\gamma_\perp+\kappa)}{2}\pm\frac{i\kappa}{2}[8Cq-(1-q)^2]^{1/2} . \quad (59)$$

The spectrum exhibits sidepeaks, with positions dependent on C. This is in contrast to the high-Q and low-Q adiabatic elimination spectra which never show sidepeaks in the absorptive limit for intensities below saturation (of course at saturation intensities the low-Q absorptive spectrum shows the three-peak Stark splitting with sidepeaks at $\omega=\pm\gamma_\perp\sqrt{2I}$). The sidepeaks in this zero-intensity limit arise because of a splitting in the degenerate first-excited energy level of the atom-field system.[26] This vacuum-field Rabi splitting was discussed by Sanchez-Mondragon, Narozhny, and Eberly[28] who considered a Rydberg atom interacting with a single mode of a lossless cavity. The system is modelled by the Hamiltonian

$$H=\hbar g(\sigma a^\dagger+\sigma^\dagger a)+\hbar\omega_0 a^\dagger a+\tfrac{1}{2}\hbar\omega_0\sigma_z . \quad (60)$$

It is well known that the degenerate eigenstate with energy $\hbar\omega_0(n+1)$ is split by the atom-field interaction. The energy splitting is $\pm\hbar\Omega/2$, where $\Omega=2g\sqrt{n+1}$ (Fig. 4). The first excited state is split by $\pm\hbar g$. The spectrum calculated by Sanchez-Mondragon, Narozhny, and Eberly shows side peaks at the frequencies $\pm g$. Agarwal[29,53] showed the effect to be cooperative. With N atoms the splitting increases to $\pm g\sqrt{N}$. The vacuum-field Rabi spitting is not observable for the situation of a radiatively damped atom. However, Carmichael[26] has pointed out that the splitting might be evidenced at optical frequencies by placing the atoms in a cavity with a relaxation time comparable to that of the atomic damping. He shows that the system in the low-intensity limit may be modelled as a pair of damped coupled harmonic oscillators representing the field and atomic polarization. The normal modes of vibration in the nondamped situation oscillate at frequencies $\omega_L\pm g\sqrt{N}$. This corresponds to a splitting [Fig. 5(a)] of $\pm g\sqrt{N}$ in the degenerate first excited state of the atom-field system. This may be recognized in Eq. (3) by noting that in the low-intensity limit, $D=-N$ and the resulting coupled equations in α and v correspond to the linearized equations (6) in the limit $\alpha_0=0$ and $D_0=-N$. These equations have eigenvalues given by (56), which in the nondissipative limit ($\gamma_\perp=\gamma_\parallel=\kappa=0$) are $\pm ig\sqrt{N}$. Carmichael then includes damping in his model and shows the splitting effect to be optimized for $\gamma_\perp=\kappa$, the normal modes being decoupled and independently damped and the frequencies of oscillation still $\omega_L\pm g\sqrt{N}$. For the more general case $\gamma_\perp\neq\kappa$, the normal modes are coupled and the new term $(1-q)^2$ appearing in (59) will eventually destroy the vacuum-field Rabi splitting as the ratio $\gamma_\perp/\kappa$ becomes too large or too small.[26] The vacuum-field splitting has now been experimentally evidenced both in Rydberg atoms[54] and in the system of optical bistability.[55,27]

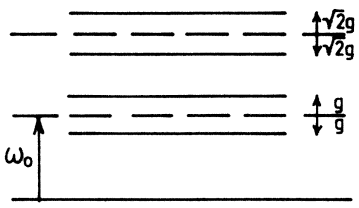

FIG. 4. The dressed states for a single atom interacting with a cavity mode ($\omega_L=\omega_0=\omega_C$ and $\gamma_\perp=\gamma_\parallel=\kappa=0$). The splitting of the first and second excited states are shown.

Figure 5 plots the intensity and squeezing spectra in the absorptive situation, where $\Delta=\phi=0$, for various q and C values. The vacuum-field Rabi splitting is clearly apparent in Figs. 5(b) and 5(c) for low-intensity regime and $q\sim 1$, in accordance with the eigenvalues (59). We notice increased squeezing at these sidepeaks.[5,27] The increase occurs because of the scattering process depicted in Fig. 5(a) where there is enhancement of coupling between frequencies $\omega_L+g\sqrt{N}$ and $\omega_L-g\sqrt{N}$. For larger q values the linewidth is greater than the splitting, the doublet is not resolved, and the vacuum-field splitting is not evident.

Of particular interest to us in this paper is the behavior of the spectra including nonzero atomic and cavity detunings. The effect of vacuum-field splitting in the dispersive situation has been discussed and experimentally investigated by Raizen *et al.*[5] and Orozco *et al.*,[27] and the reader is referred to these works. We study in the first instance the situation of equal cavity and atomic frequencies ($\omega_0=\omega_c$, $\kappa\phi=\gamma_\perp\Delta$, or $q=\phi/\Delta$). We find the eigenvalues (56) in the low-intensity limit to be precisely

$$\begin{aligned}\mathrm{Re}\lambda_{2,3}&=-\frac{(\gamma_\perp+\kappa)}{2} ,\\ \mathrm{Im}\lambda_{2,3}&=-\kappa\phi\pm\kappa\left[2Cq-\frac{(1-q)^2}{4}\right]^{1/2}\\ &=-(\omega_0-\omega_L)\pm\left[g^2N-\frac{(\kappa-\gamma_\perp)^2}{4}\right]^{1/2} .\end{aligned} \quad (61)$$

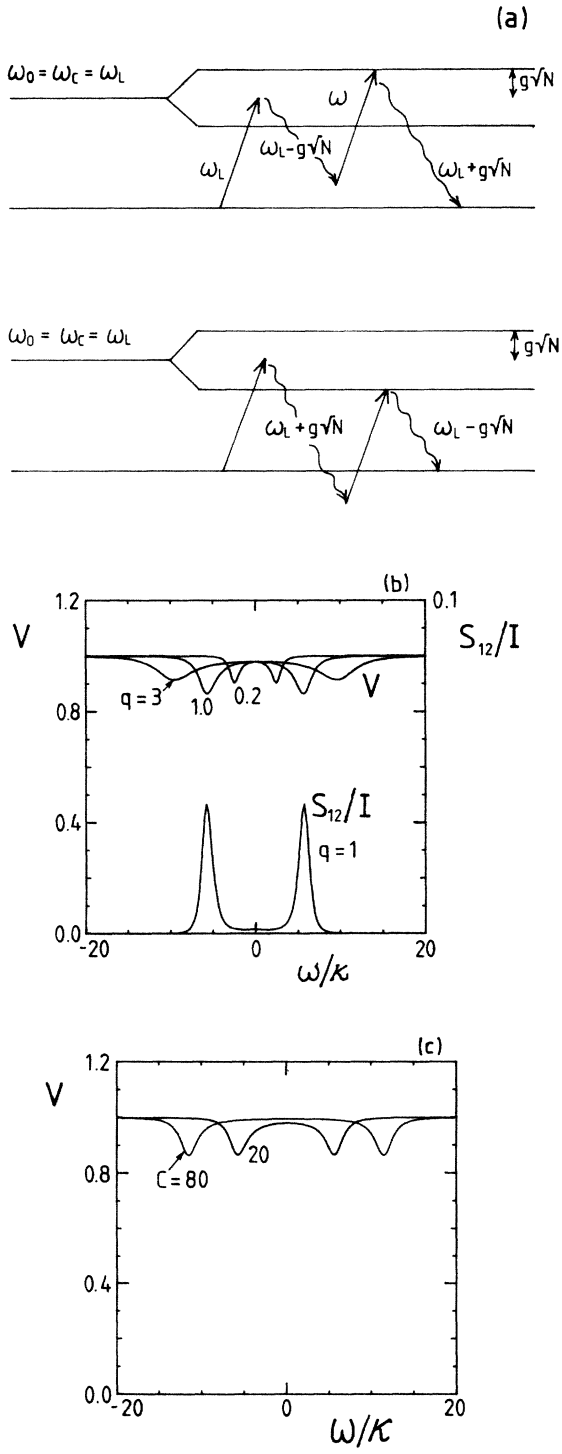

FIG. 5. Vacuum-field splitting in the absorptive limit. (a) Scattering processes give rise to sidepeaks in the spectrum at frequencies $\omega_L \pm g\sqrt{N}$ (for $\gamma_\perp=\kappa$). (b) Vacuum-field Rabi splitting is evident in the squeezing $V(X_\theta,\omega)$ and incoherent intensity spectra $S_{12}(\omega)/I$, for intermediate q values. $\Delta=\phi=0$, $C=20$, $I=2$, $f=1$, $n_{\rm th}=0$. [Only the incoherent part $S_{12}(\omega)$ of the intensity spectrum is plotted, the δ-function component at $\omega=0$ is not displayed.] (c) Vacuum-field Rabi splitting. Squeezing spectrum $V(X_\theta,\omega)$ plotted for $\Delta=\phi=0$, $I=2$, $q=1$, $f=1$, $n_{\rm th}=0$, and for various cavity cooperativity C.

This suggests a splitting by

$$\pm\left[g^2N-\frac{(\kappa-\gamma_\perp)^2}{4}\right]^{1/2}.$$

Thus for the situation where $8Cq \gg (1-q)^2$ one has sufficient cavity cooperativity that vacuum-field Rabi splitting may be evidenced. There are now four sidepeaks in the spectrum, at approximately $\omega_L \pm (\omega/\kappa)$, where $(\omega/\kappa)=-\kappa\phi\pm\kappa\sqrt{2Cq}$. The relevant scattering processes are depicted Fig. 6(a), which illustrates the particular case where the pump frequency is almost resonant with the dressed energy state: $\omega_L \sim \omega_0 - g\sqrt{N}$ (i.e., $\kappa\phi \sim \kappa\sqrt{2Cq}$ or $\phi \sim 2C/\Delta$). For this choice of ϕ, we have sidepeak pairs well separated in frequency, at $|\omega| \sim 0$ and $|\omega| \sim 2\kappa\phi$. The splitting $\pm\kappa\sqrt{2Cq}$ about the positions $\pm\kappa\phi$ is vacuum-field Rabi splitting and is predicted to increase with C. The squeezing spectrum for a situation of this type is depicted in Fig. 6(b), for $C=1100$, $I=300$, $\Delta=100$, and $\phi=18$. The value $q=0.18$ corresponds to $\omega_0=\omega_c$, and we see indeed four sidepeaks (vacuum Rabi splitting). The outer sidepeaks are a long way detuned from the pump frequency and show considerably less squeezing than the inner peaks. This might be expected since [Fig. 6(a)] the scattered photon at $\omega_L-\kappa\phi-g\sqrt{N}$ is a long way from resonance with any of the transitions between the dressed energy levels. Figure 6(c) plots the spectra for varying q values (note now $\omega_0 \neq \omega_c$). For sufficiently small and large q the second pair of sidepeaks vanish (vacuum-field Rabi splitting disappears). We notice that the squeezing obtainable is almost independent of q. This is a consequence of our choice of cavity detuning $\phi \sim 2C/\Delta$. The low- and high-q adiabatic situations have been described by Eqs. (45) and (54) and are depicted schematically in Figs. 3(b) and 2(b), respectively. The atomic (and cavity) energy levels are shifted by $(2C\gamma_\perp)/\phi$ [and $(2C\kappa)/\Delta$], respectively. Thus a cavity detuning $\kappa\phi \sim (2C\kappa)/\Delta$ brings the pump into resonance with the dressed levels.

Figure 7(a) illustrates the situation (61) of equal cavity and atomic frequencies ($\omega_0=\omega_c$), but with the pump frequency closer to resonance with the original cavity frequency. Thus [provided $8Cq$ is sufficiently greater than $(1-q)^2$], we see a splitting of $\pm\kappa\phi$ about the two (vacuum-field Rabi) positions at $\pm\kappa\sqrt{2Cq}$. The squeezing spectrum is plotted in Fig. 7(b) for $\Delta=8$, $C=30$, $I=10$, $\phi=1$, and $q=0.125$ (corresponding to $\omega_0=\omega_c$). The scattered photons are approximately resonant with the transitions $\omega_0 \pm g\sqrt{N}$ allowed by the dressed atomic-cavity system, and we see reasonable squeezing is possible at the inner sidepeaks, which are closer to resonance with the driving field. The squeezing will drop significantly as we change q to move close to the adiabatic elimination limits, since this case of lower cavity detuning does not allow resonance with the dressed cavity (or atomic) energy level. The low-Q adiabatic limit is shown in Fig. 7(b) ($q=0.01$).

Figure 7(c) plots squeezing spectra, for the case $\omega_0=\omega_C$ ($q=\phi/\Delta$), but with varying cavity detunings ϕ. The best squeezing is obtained for the cavity detuning $\phi \sim 2C/\Delta$ (discussed above in Fig. 6) where the driving

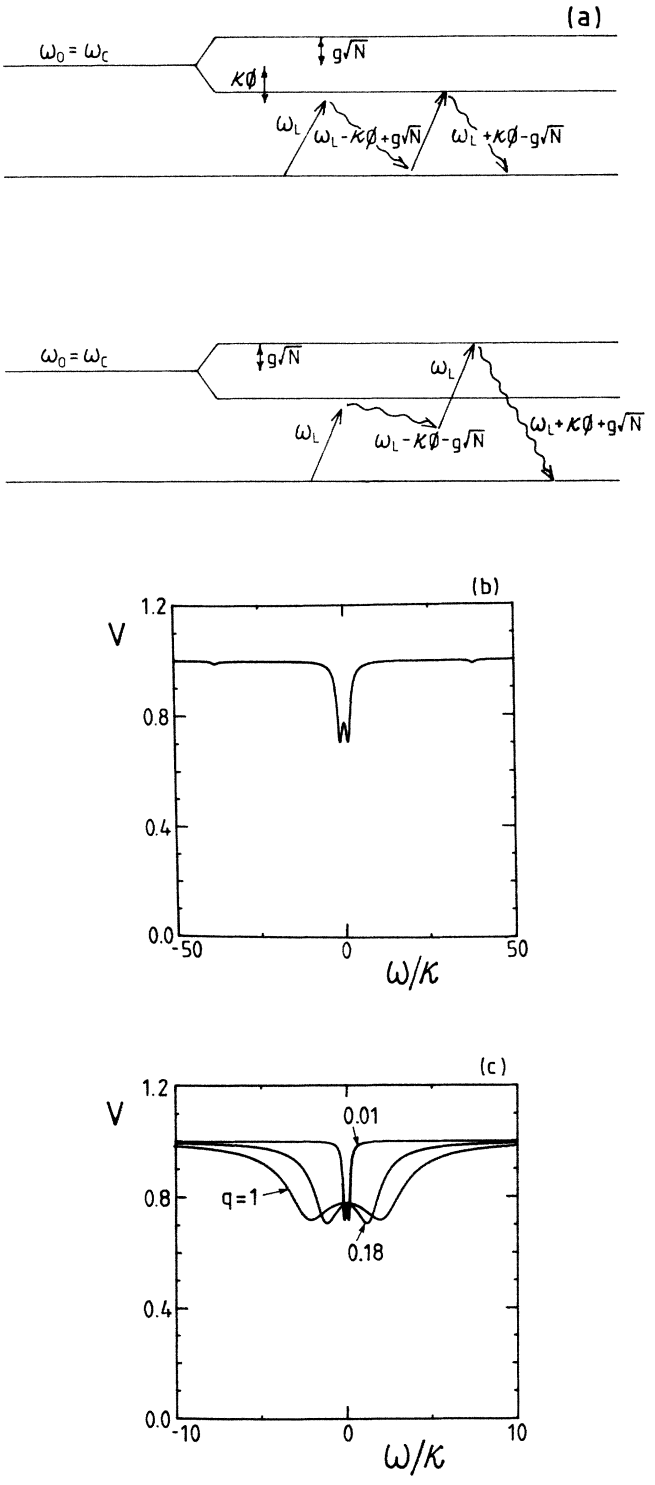

FIG. 6. (a) Vacuum-field Rabi splitting for $\omega_0=\omega_C\neq\omega_L$. We have taken the case $g^2N\gg(\kappa-\gamma_\perp)^2/4$. The two possible scattering processes are depicted, giving rise to two pairs of sidepeaks in the spectrum. The pump is tuned close to resonance with the dressed energy level. (b) Squeezing spectrum $V(X_\theta,\omega)$ for $\Delta=100$, $C=1100$, $\phi=18$, $I=300$, $f=1$ $n_{\rm th}=0$, $q=0.18$. Two pairs of sidepeaks are apparent, due to the vacuum-field Rabi splitting depicted in (a). (c) $V(X_\theta,\omega)$. $\Delta=100$, $C=1100$, $\phi=18$, $I=300$, $f=1$, $n_{\rm th}=0$. Various q values.

field is resonant with the dressed energy level. Figure 7(d) plots for $\Delta=8$, $C=30$, $I=10$, and $\phi=6$ the squeezing spectra for various q values, again showing the independence of the best squeezing obtainable on q, if $\phi\sim 2C/\Delta$.

The more general situation (also depicted in Figs. 6 and 7) involves nonequal cavity and atomic frequencies ($\omega_0\neq\omega_C$ or $q\neq\phi/\Delta$). For sufficient cooperativity C that

$$g\sqrt{N}\gg\frac{|\gamma_\perp-\kappa|}{2}$$

and

$$g\sqrt{N}\gg\left|\left|\frac{(\gamma_\perp-\kappa)}{2}\frac{(\omega_0-\omega_C)}{2}\right|\right|^{1/2},$$

the eigenvalues are approximately

$$\begin{aligned}\mathrm{Re}\lambda_{2,3}&=-\frac{(\gamma_\perp+\kappa)}{2},\\ \mathrm{Im}\lambda_{2,3}&=\omega_L-\frac{(\omega_0+\omega_C)}{2}\pm\left[g^2N+\left[\frac{\omega_0-\omega_C}{2}\right]^{1/2}\right.\\ &=-\frac{\kappa(\phi+q\Delta)}{2}\pm\kappa\left[2Cq+\left[\frac{\phi-q\Delta}{2}\right]^2\right]^{1/2}.\end{aligned}\tag{62}$$

The scattering processes are illustrated in Fig. 7(e), and an example of the squeezing spectrum is plotted in Fig. 7(b) for $q=0.7$. We notice good squeezing possible for the innermost peak [corresponding to the second diagram of Fig. 7(e)].

An interesting situation enabling a enhancement of scattering processes (and hence strong squeezing) is where the cavity is detuned oppositely to the atoms ($\phi/\Delta<0$, as in Fig. 8) and the laser is tuned to $(\omega_0+\omega_C)/2$ (i.e., $q=-\phi/\Delta$). With sufficient cavity cooperativity C that (62) holds, we have

$$\begin{aligned}\mathrm{Re}\lambda_{2,3}&=\frac{-(\gamma_\perp+\kappa)}{2},\\ \mathrm{Im}\lambda_{2,3}&=\pm\left[g^2N+\frac{(\omega_0-\omega_C)^2}{4}\right]^{1/2}\\ &=\pm\kappa(2Cq+\phi^2)^{1/2}.\end{aligned}\tag{63}$$

The imaginary parts of two pairs of eigenvalues coincides and we see a single pair of sidepeaks at

$$\omega=\pm\left[g^2N+\frac{(\omega_0-\omega_C)^2}{4}\right]^{1/2}$$

(vacuum-field Rabi splitting). This corresponds to a single doubly resonant scattering as depicted in Fig. 8(a). The squeezing spectrum is plotted for $\Delta=8$, $C=30$, $I=10$, $q=0.125$, and $\phi=-1$ in Fig. 8(b). For higher q values, we again see two pairs of sidepeaks, split from the

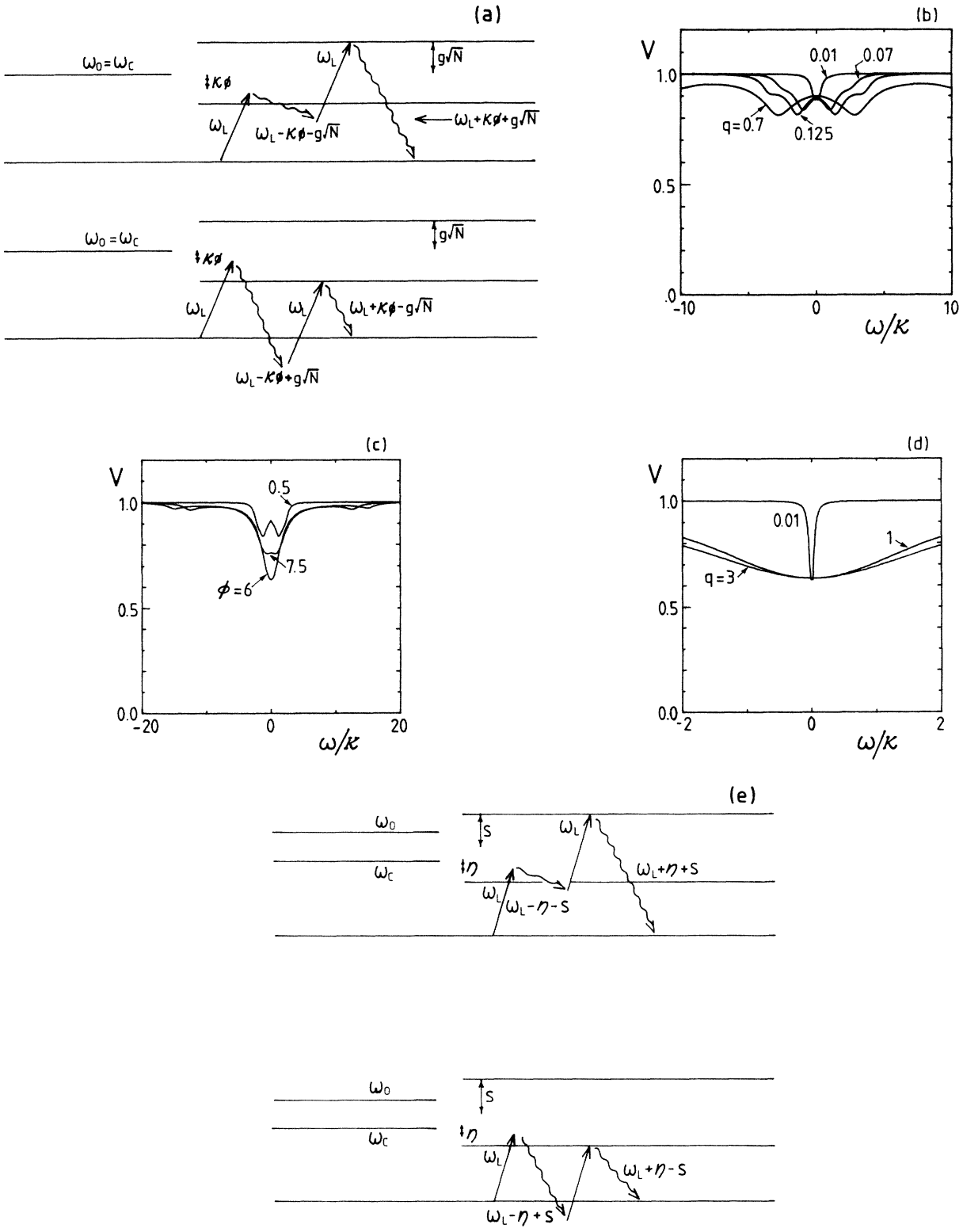

FIG. 7. (a) Vacuum-field Rabi splitting for $\omega_0=\omega_C\neq\omega_L$. As in Fig. 6(a), but the pump is tuned close to resonance with ω_0. (b) Squeezing spectra $V(X_\theta,\omega)$ for the situation corresponding to (a). $\Delta=8$, $C=30$, $I=10$, $\phi=1$, $f=1$, $n_{\rm th}=0$, and $q=0.125$. Other values of q (such that $\omega_0\neq\omega_C$) are also plotted. (c) $V(X_\theta,\omega)$ for the situation depicted in Figs. 6(a) and 7(a) where $\omega_0=\omega_C$, but for various cavity detunings ϕ. $\Delta=8$, $C=30$, $I=10$, $f=1$, and $n_{\rm th}=0$. (d) $V(X_\theta,\omega)$. $\Delta=8$, $C=30$, $\phi=6$, $f=1$, $I=10$, and $n_{\rm th}=0$. Various q values. (e) Vacuum-field Rabi splitting for $\omega_0\neq\omega_C\neq\omega_L$. We have taken large $g\sqrt{N}$ as in Eq. (62). An example of the squeezing spectrum in this case is (b), $q=0.7$. $S=[g^2N+(\omega_0-\omega_C)^2/4]^{1/2}$, $\eta=\kappa\phi+\gamma_\perp\Delta$.

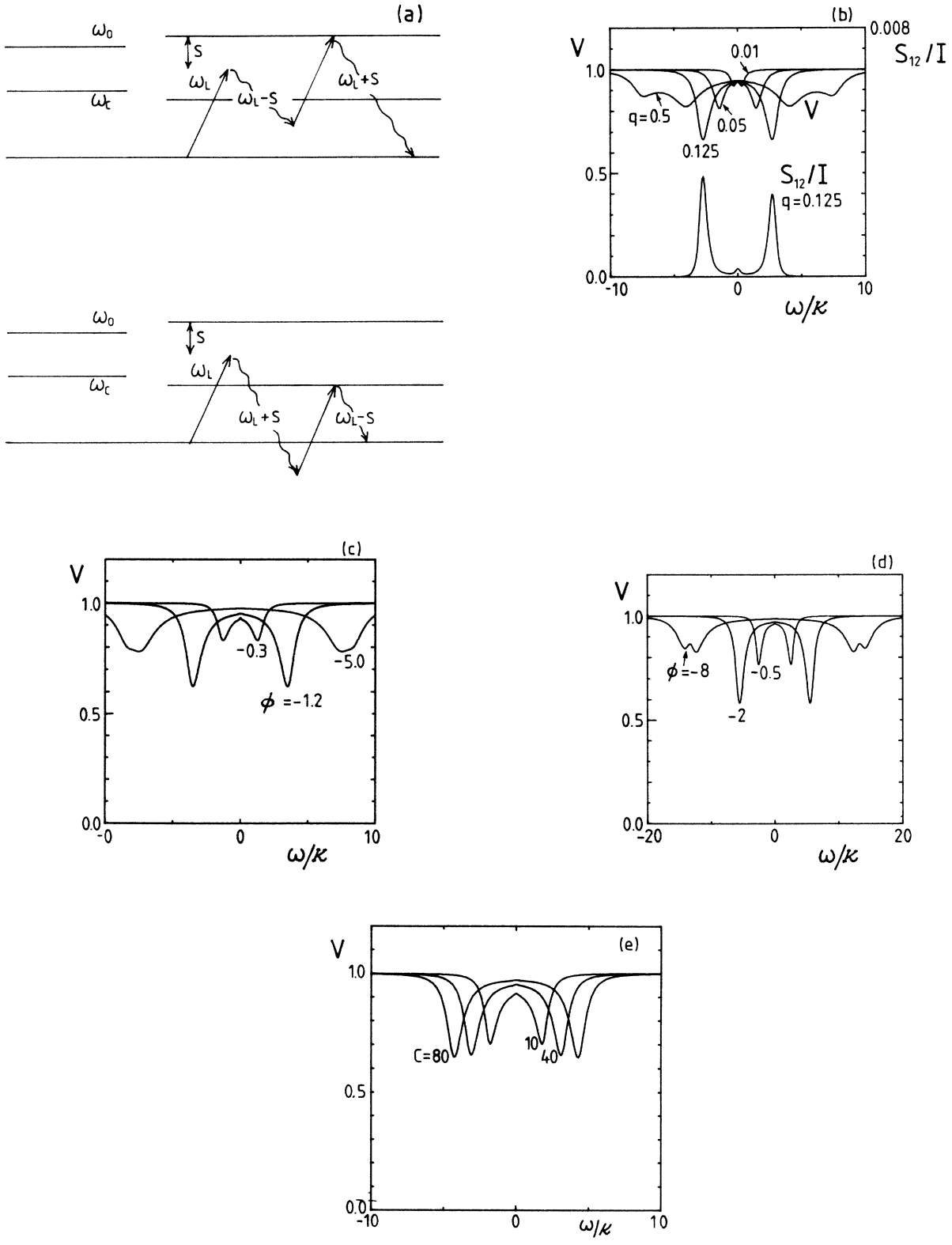

FIG. 8. (a) Vacuum-field splitting for $\omega_L=(\omega_0+\omega_C)/2$. S is defined in Fig. 7(e). The processes depicted reinforce and give rise to spectral sidebands at frequencies $\omega_L \pm S$. (b) Squeezing $V(X_\theta,\omega)$ and incoherent intensity $S_{12}(\omega)$ for the situation depicted in Fig. 7(a): $\Delta=8$, $\phi=-1$, $I=10$, $C=30$, $f=1$, $n_{\rm th}=0$, $q=0.125$. Also plotted are spectra for $q=0.01,0.05,0.5$. The optimal phase angle for $q=0.125$ is $\theta=127°$, at $\omega/\kappa=2.7$. (c) $V(X_\theta,\omega)$ for the resonant situation $\omega_L=(\omega_0+\omega_C)/2$ depicted in (a). $\Delta=8$, $C=30$, $I=10$, $f=1$, $n_{\rm th}=0$. Various ϕ are plotted. $q=-\phi/\Delta$. (d) $V(X_\theta,\omega)$ for $\Delta=8$, $C=60$, $I=10$, $f=1$, $n_{\rm th}=0$, and $q=-\phi/\Delta$. (e) $V(X_\theta,\omega)$ for $\Delta=8$, $I=10$, $f=1$, $n_{\rm th}=0$, $\phi=-1.2$, $q=-\phi/\Delta$.

position $(2Cq+\phi^2)^{1/2}$ by $\kappa(\phi+q\Delta)$ in agreement with (62). There is reduced squeezing as the resonance is lost. Figure 8(c) shows squeezing spectra for $\Delta=8$, $C=30$, $I=10$, and various cavity detunings ϕ, where one has in each case the situation depicted in Fig. 8(a), $q=-\phi/\Delta$ for resonance with both transitions. Squeezing reduces as ϕ^2 becomes comparable to $2Cq$ and as we approach the adiabatic elimination limits. Figure 8(d) plots the squeezing spectra for a higher value of C ($C=60$), showing good squeezing to be obtainable for greater cavity detunings ϕ. Figure 8(e) shows squeezing spectra for a range of C values. The squeezing in this case of $\phi/\Delta<0$ is perhaps only somewhat better than that obtainable if one selects an optimal cavity detuning ϕ of the same sign as Δ [as in Fig. 7(d)]. The enhancement, however, provides evidence for vacuum-field splitting. Enhancement of squeezing in this vacuum-field splitting regime has been experimentally demonstrated by Raizen *et al.*[5]

We wish to demonstrate in Fig. 9 the effect of varying the cavity cooperativity C relative to the detunings $\omega_0-\omega_C$, for a fixed ratio of decay rates $q=\gamma_\perp/\kappa$. The low-intensity solution for $q=1$, (i.e., $\gamma_\perp=\kappa$) is exactly

$$\mathrm{Im}\lambda_{2,3}=\omega_L-\left[\frac{\omega_0+\omega_C}{2}\right] \pm\left[g^2N+\frac{(\omega_0-\omega_C)^2}{4}\right]^{1/2},$$
$$\mathrm{Re}\lambda_{2,3}=-\kappa\ . \tag{64}$$

Thus for

$$g^2N\gg\frac{(\omega_0-\omega_C)^2}{4},\quad\left[2C\gg\frac{(\phi-\Delta)^2}{4}\right]$$

we see the vacuum-field Rabi-splitting doublet at $\pm g\sqrt{N}$ [split by $(\omega_0+\omega_C)/2-\omega_L$] [Fig. 9(a)]. In the other limit of large $\omega_0-\omega_C$ relative to $g\sqrt{N}$, we see the usual fluorescence peaks at the cavity and atomic resonance ω_0, ω_C, respectively,

$$\mathrm{Im}\lambda_2=\omega_L-\omega_C,\quad \mathrm{Im}\lambda_3=\omega_L-\omega_0$$

[Fig. 9(b)]. We notice the effect of the thermal-type noise Λ (discussed in Sec. VI) in enhancing the intensity at the resonance $\omega_L+\eta-s$ of Fig. 7(e).

The spectra for higher values of intensity I are illustrated in Fig. 10. We point out that to get squeezing at all one requires nonzero intensity, and possibilities of good squeezing often improve with intensity. As the intensity is increased, transitions between the higher excited states of the dressed atom-field system occur [cf. Figs. 4 and 1(d)]. This is evidenced as an extra peak at $\omega=0$ in the spectra. The appearance of a central fluorescence peak is evidenced in Fig. 10(a). For such intensities, the high-Q adiabatic solution exhibits increased noise (and no squeezing) at the sidepeaks corresponding to the cavity resonance ω_c' and $2\omega_L-\omega_C'$ [Fig. 2(e)]. This noise is due to the thermal-type fluorescence $\Lambda(0)$ [central Rabi peak of the atomic fluorescence spectrum $\Lambda(\bar{\omega})$ of Fig. 1(e)] and has been discussed in Sec. VI. For relatively "high"-q values the resonance frequency will fall within the center peak and the squeezing and intensity spectra will show the features of the high-Q adiabatic elimination spectra discussed in Sec. VI. For lower-Q values ($q\lesssim 1$), however, the resonance corresponds to frequencies well outside the atomic linewidth and squeezing is possible at resonances of the type depicted in Figs. 2(b) and 8(a). We notice in Fig. 10(a) the sidepeaks for this moderate intensity have essentially the width and position indicated by the vacuum-field splitting [Eq. (62)]. Figure 10(b) plots spectra for still higher values of intensity. The positions of the sidepeaks (barely visible) indicate Stark splitting as I becomes sufficiently large relative to C [Fig. 10(c)]. Figures 10(d) and 10(e) make comparisons with spectra possible for lower-q values approaching the low-Q limit.

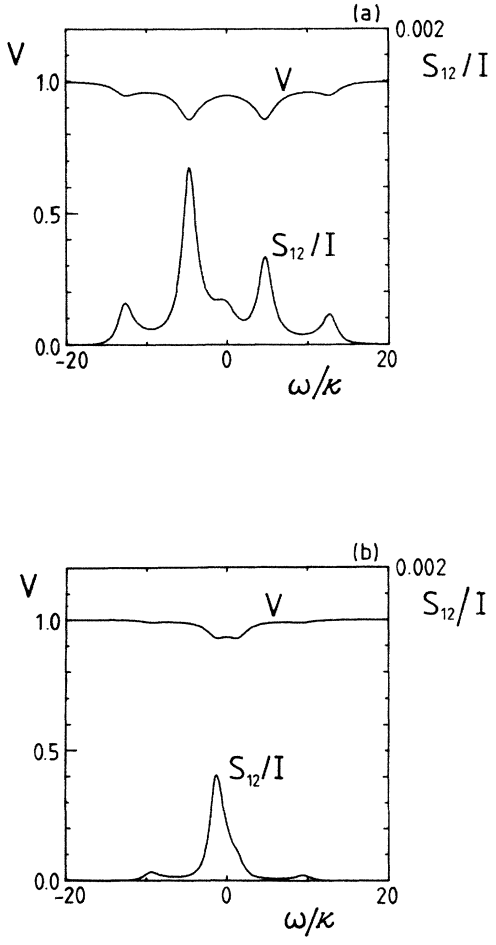

FIG. 9. Squeezing $V(X_\theta,\omega)$ and intensity $S_{12}(\omega)$ spectra for $\gamma_\perp=\kappa$: $\Delta=8$, $\phi=-1$, $I=10$, $(\omega_0-\omega_C=9\kappa)$. (a) $C=30$. (b) $C=3$.

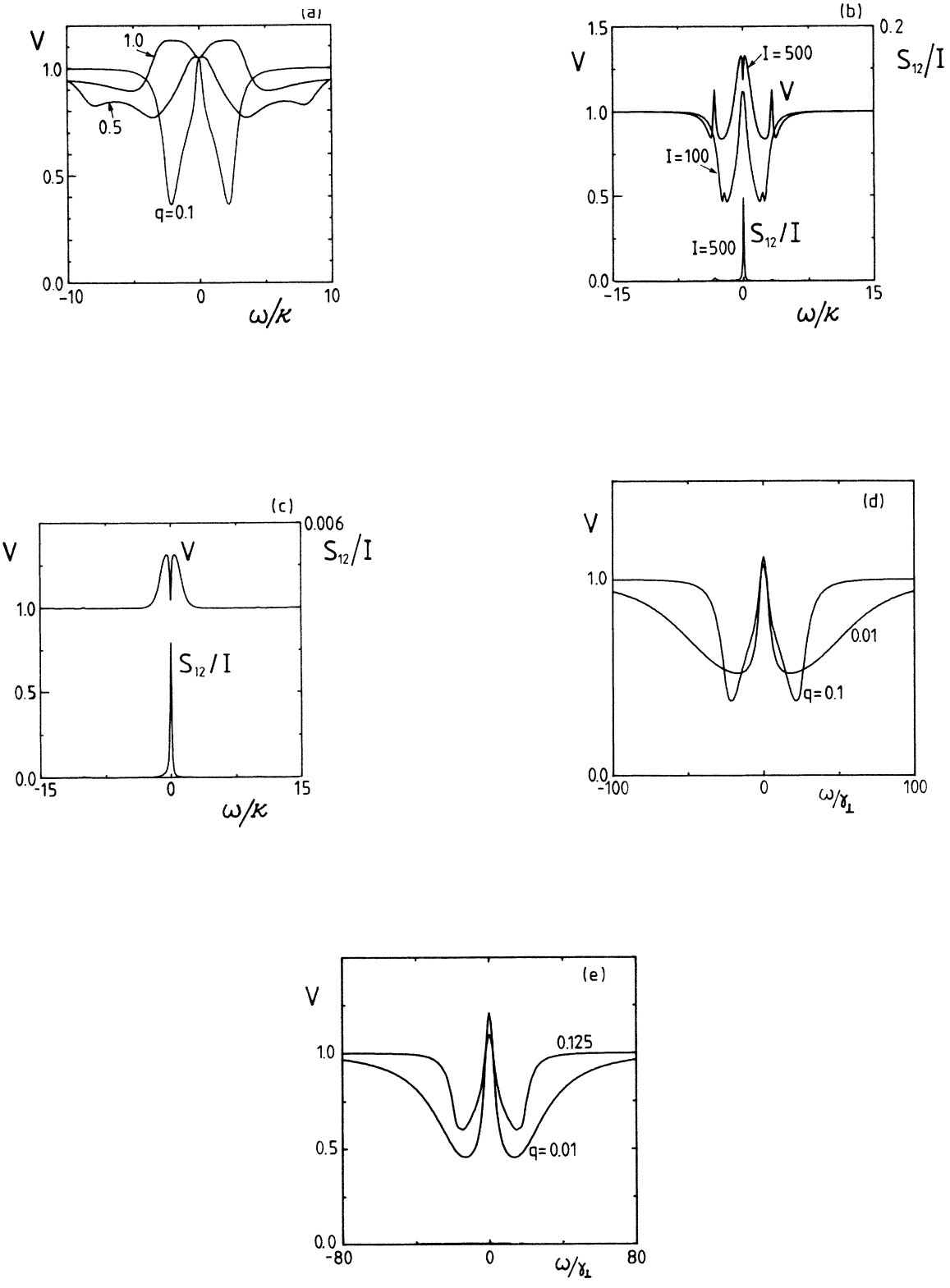

FIG. 10. Spectra at higher intensities: (a) $V(X_\theta,\omega)$ for $\Delta=8$, $C=30$, $C=30$, $\phi=-1$, $f=1$, $n_{\rm th}=0$, $I=50$. Various $q=\gamma_\perp/\kappa$. The noise due to scattering of photons at $\omega=0$ is apparent. (b) $V(X_\theta,\omega)$ for various intensities. $\Delta=8$, $C=30$, $\phi=-1$, $f=1$, $n_{\rm th}=0$, $q=0.1$. (c) Squeezing and intensity spectra for $\Delta=8$, $C=30$, $\phi=-1$, $f=1$, $n_{\rm th}=0$, $q=0.1$, $I=5000$. (d) $V(X_\theta,\omega)$ for $\Delta=8$, $I=64$, $C=30$, $f=1$, $n_{\rm th}=0$. The curve $q=0.1$ has $\phi=-1$. The curve $q=0.01$ has $\phi=0$ and approaches the low-Q limit. (e) $V(X_\theta,\omega)$ for $\Delta=8$, $I=64$, $C=10$, $f=1$, $n_{\rm th}=0$. The two curves correspond to parameters ($q=0.125$, $\phi=-1$) and ($q=0.01$, $\phi=0$).

Similar orders of squeezing are obtainable. The mechanism for squeezed sidepeaks is a Rabi splitting increasing with both C and I. The lower-q values become more sensitive to the splitting in I and may become advantageous for lower C values [cf. Figs. 10(d), 10(e), 3(f), and 7(e)].

IX. CONCLUSION

We have presented a quantum theory of N two-level atoms in an optical cavity without adiabatic elimination of cavity or atomic variables. The theory is based on the linearized equations derived by Drummond and Walls in the positive P representation. The solution for the stationary transmitted spectrum of fluctuations is that obtained previously in the high-Q limit but with the atomic coefficients showing a frequency dependence. The transmitted squeezing and intensity spectra are calculated and include atomic and cavity detunings. The solutions are analytical and are explicit functions of the cavity and atomic parameters.

The spectra are discussed both in the high-Q and low-Q adiabatic elimination limits. The high-Q adiabatic elimination spectra shows sensitivity at higher intensities to the phase insensitive atomic fluorescence noise corresponding to the center peak of the Stark triplet. The atomic noise is broadband compared to the narrow-cavity linewidth, and the intensity spectrum shows asymmetric side peaks with enhancement at the cavity resonance. The spectrum of quadrature phase fluctuations thus reveals increased noise (considerably reduced or no squeezing) at these higher intensities. The broadening of the cavity linewidth relative to the atomic linewidth means the low-Q adiabatic elimination spectrum shows three peaks at higher intensities due to the Stark splitting of the atomic energy levels. Good squeezing is possible at the sidepeaks of the spectrum because of resonantly enhanced mixing.

The spectra without adiabatic elimination are also discussed. The spectra may exhibit vacuum-field Rabi splitting, for sufficiently high-cavity cooperativity C (or $g\sqrt{N}$), as pointed out by Carmichael[26] and Raizen *et al.*[5] The splitting is at low intensities and increases with the factor $g\sqrt{N}$. We have solved for the eigenvalues in the low-intensity limit. For the case of equal cavity and atomic frequencies, one observes four sidepeaks in the spectrum at low intensities. The squeezing at these sidepeaks is enhanced, and the effect of the cavity detuning on the order of squeezing obtainable is discussed. We examine also the more general case of nonequal atomic and cavity frequencies. Good squeezing is obtainable over a broad parameter range, with appropriate choice of cavity detuning. Particularly interesting is the situation where the pump is tuned midway between the atom and cavity resonance [$\omega_L=(\omega_0+\omega_C)/2$]. The sidepeak pairs coalesce, and we observe (for sufficient cavity cooperativity C) a single pair of side peaks at frequencies $\omega_L \pm g\sqrt{N}$. Squeezing obtained in this case is strong because of the resonant scattering depicted in Fig. 8(a). The effect of cavity detuning (and relative decay rates $q=\gamma_\perp/\kappa$) on the squeezing is discussed.

We also present results for higher intensities. The higher q values ($q \gtrsim 1$) show less squeezing at greater intensities being sensitive to the phase-insensitive fluorescence, which dominates over a central frequency band at higher intensities. The employment of lower $\gamma_\perp/\kappa$ ratios and a suitably tuned laser, however, allows excellent squeezing to be obtained at higher intensities in the wings of the spectrum. The mechanism for squeezed sidepeaks is a general Rabi splitting of the dressed cavity-atom energy levels.

ACKNOWLEDGMENTS

The author is grateful to A. Lane, D. F. Walls, M. Marte, P. Drummond, M. Raizen, M. Xiao, and H. J. Kimble for stimulating conversations regarding this work.

[1]R. E. Slusher, L. W. Hollberg, B. Yurke, J. C. Metz, and J. F. Valley, Phys. Rev. Lett. **55**, 2409 (1985).
[2]R. M. Shelby, M. D. Levenson, S. H. Perlmutter, R. S. DeVoe, and D. F. Walls, Phys. Rev. Lett. **57**, 691 (1986).
[3]M. W. Maeda, P. Kumar, and J. H. Shapiro, Opt. Lett. **12**, 161 (1987).
[4]L. Wu, H. J. Kimble, J. L. Hall, and H. Wu, Phys. Rev. Lett. **57**, 2520 (1986).
[5]M. G. Raizen, L. Orozco, M. Xiao, T. L. Boyd, and H. J. Kimble, Phys. Rev. Lett. **59**, 198 (1987).
[6]S. Machida, Y. Yamamoto, and J. Itaya, Phys. Rev. Lett. **58**, 1000 (1987).
[7]D. Stoler, Phys. Rev. D **1**, 3217 (1970).
[8]H. P. Yuen, Phys. Rev. A **13**, 2226 (1976).
[9]C. M. Caves, Phys. Rev. D **23**, 1693 (1981).
[10]G. S. Agarwal, L. M. Narducci, R. Gilmore, and Da Hsuan Feng, Phys. Rev. A **18**, 620 (1978).
[11]G. S. Agarwal and S. P. Tewari, Phys. Rev. A **21**, 1638 (1980).
[12]L. A. Lugiato, Nuovo Cimento B **50**, 89 (1979).
[13]F. Casagrande and L. A. Lugiato, Nuovo Cimento B **55**, 173 (1980).
[14]L. A. Lugiato, F. Casagrande, and L. Pizzuto, Phys. Rev. A **26**, 3438 (1982).
[15]P. D. Drummond and D. F. Walls, Phys. Rev. A **23**, 2563 (1981).
[16]M. Sargent III, D. A. Holm, and M. Zubairy, Phys. Rev. A **31**, 3112 (1985); S. Stenholm, D. A. Holm, and M. Sargent III, *ibid.* **31**, 3124 (1985); M. Sargent III, M. O. Scully, and W. E. Lamb, Jr., *Laser Physics* (Addison-Wesley, Reading, MA, 1974).
[17]L. A. Lugiato, in *Progress in Optics XXI*, edited by E. Wolf (North-Holland, Amsterdam, 1984).
[18]L. A. Lugiato and G. Strini, Opt. Commun. **41**, 67 (1982).
[19]M. D. Reid and D. F. Walls, Phys. Rev. A **33**, 4465 (1986).
[20]M. D. Reid and D. F. Walls, Phys. Rev. A **34**, 4929 (1986).
[21]D. A. Holm, M. Sargent III, and B. A. Capron, Opt. Lett. **11**, 443 (1986).
[22]D. A. Holm and M. Sargent III (to be published).
[23]S. Ho, P. Kumar, and J. H. Shapiro, Phys. Rev. A **35**, 3982 (1987).

[24]R. E. Slusher, B. Yurke, P. Grangier, D. F. Walls, and M. D. Reid, J. Opt. Soc. Am. B **4**, 1453 (1987).
[25]M. D. Reid, A. Lane, and D. F. Walls, in *Quantum Optics IV,* edited by J. D. Harvey and D. F. Walls (Springer, Berlin, 1986).
[26]H. J. Carmichael, Phys. Rev. A **33**, 3262 (1986).
[27]L. A. Orozco, M. G. Raizen, M. Xiao, R. J. Brecha, and H. J. Kimble, J. Opt. Soc. Am. B **4**, 1490 (1987).
[28]J. J. Sanchez-Mondragon, N. B. Narozhny, and J. H. Eberly, Phys. Rev. Lett. **51**, 551 (1983).
[29]G. S. Agarwal, Phys. Rev. Lett. **53**, 1732 (1984).
[30]H. J. Carmichael, D. F. Walls, P. D. Drummond, and S. S. Hassan, Phys. Rev. A **27**, 3112 (1983).
[31]M. D. Reid and D. F. Walls, Phys. Rev. A **32**, 396 (1985).
[32]P. D. Drummond and C. W. Gardiner, J. Phys. A **13**, 2353 (1980).
[33]H. Haken, in *Light and Matter,* Vol. XXV of *Handbüch der Physik,* edited by L. Genzel (Springer-Verlag, Berlin, 1970).
[34]R. Bonifacio and L. A. Lugiato, Lett. Nuovo Cimento **21**, 517 (1978); Phys. Rev. Lett. **40**, 1023 (1978); Phys. Rev. A **18**, 1129 (1978).
[35]M. J. Collett and C. W. Gardiner, Phys. Rev. A **30**, 1386 (1984).
[36]C. W. Gardiner and M. J. Collett, Phys. Rev. A **31**, 3761 (1985).
[37]M. J. Collett and D. F. Walls, Phys. Rev. A **32**, 2887 (1985).
[38]B. Yurke, Phys. Rev. A **29**, 408 (1984); Phys. Rev. A **32**, 300 (1985).
[39]C. M. Caves and B. L. Schumaker, Phys. Rev. A **31**, 3068 (1985).
[40]B. L. Schumaker and C. M. Caves, Phys. Rev. A **31**, 3093 (1985).
[41]M. Lax, Phys. Rev. **145**, 110 (1966).
[42]S. Chaturvedi, C. W. Gardiner, I. S. Matheson, and D. F. Walls, J. Stat. Phys. **17**, 469 (1977).
[43]C. W. Gardiner, *Handbook of Stochastic Methods in Physics, Chemistry, and Natural Sciences* (Springer-Verlag, Berlin, 1983).
[44]T. Fu and M. Sargent, Opt. Lett. **4**, 366 (1979).
[45]R. W. Boyd, M. G. Raymer, P. Narum, and D. J. Martens, Phys. Rev. A **24**, 411 (1981).
[46]K. Ikeda and O. Akimoto, Phys. Rev. Lett. **48**, 617 (1982).
[47]L. A. Lugiato, L. M. Narducci, D. K. Bardy, and C. A. Pennise, Opt. Commun. **43**, 281 (1982); **44**, 207 (1983).
[48]L. A. Lugiato, R. J. Horowicz, G. Strini, and L. M. Narducci, Phys. Rev. A **30**, 1366 (1984).
[49]L. A. Orozco, A. T. Rosenberger, and H. J. Kimble, Phys. Rev. Lett. **53**, 2547 (1984). See also L. A. Orozco, H. J. Kimble, and A. T. Rosenberger, Opt. Commun. **62**, 54 (1987).
[50]P. D. Drummond and D. F. Walls, J. Phys. A **13**, 725 (1980).
[51]M. D. Reid and D. F. Walls, Phys. Rev. A **31**, 1622 (1985).
[52]C. M. Savage and D. F. Walls, Phys. Rev. A **33**, 3282 (1986).
[53]G. S. Agarwal, J. Opt. Soc. Am. B **2**, 480 (1985).
[54]Y. Kaluzny, P. Goy, M. Gross, J. M. Raimond, and S. Haroche, Phys. Rev. Lett. **51**, 1175 (1983).
[55]R. Brecha, L. A. Orozco, M. G. Raizen, M. Xiao, and H. J. Kimble, J. Opt. Soc. Am. B **3**, 238 (1986).